Reappraising the Distributions of Energetic Electrons at Jupiter, Saturn and Uranus from Data Analyses and Physics-based Models

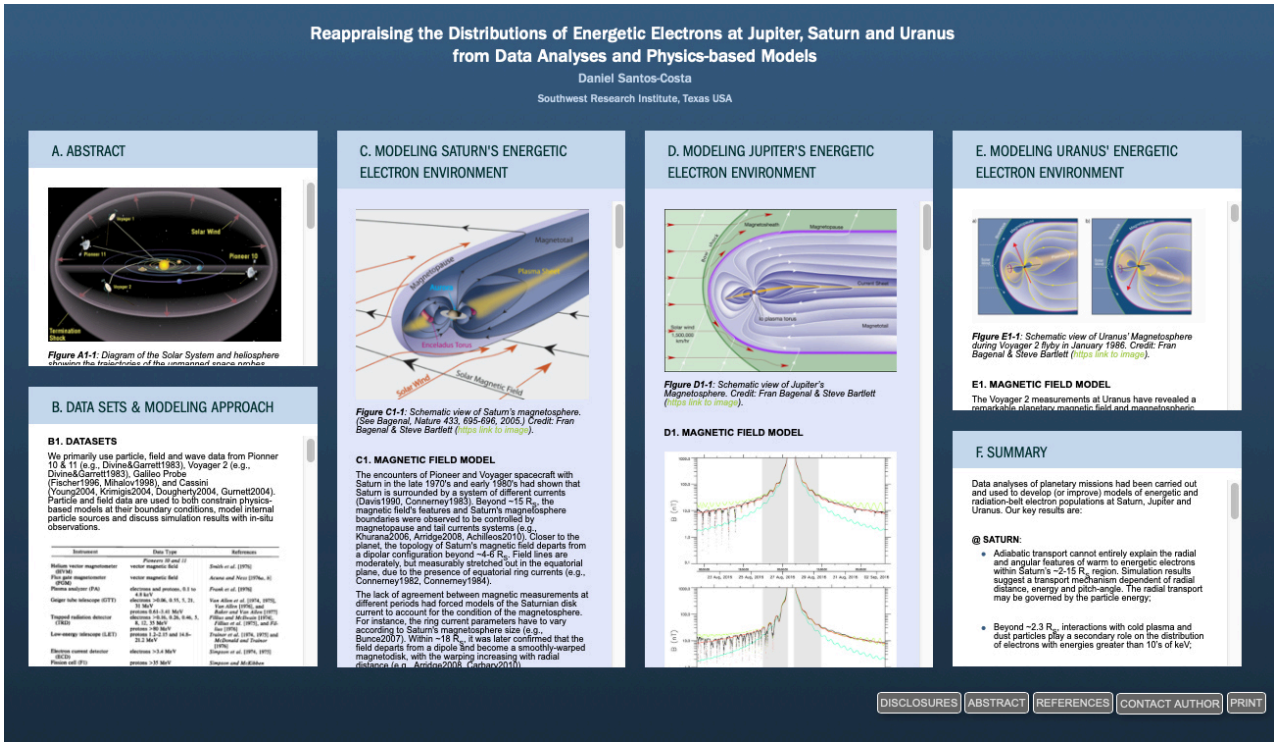

Daniel Santos-Costa

Southwest Research Institute, Texas USA

PRESENTED AT:

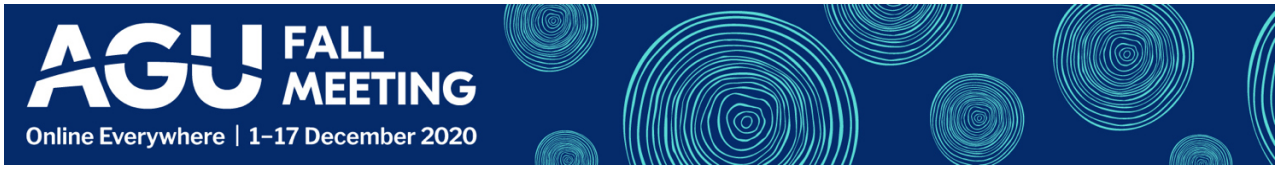

A. ABSTRACT

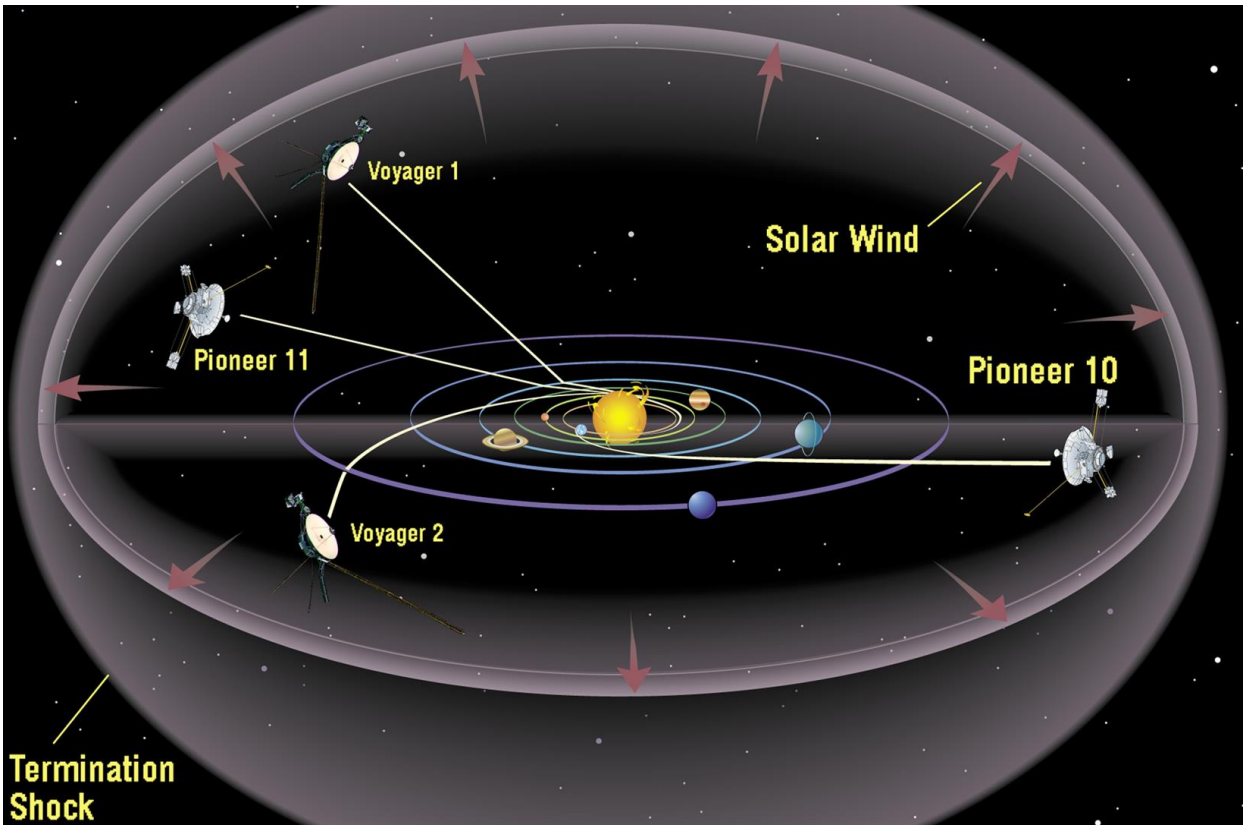

FIgure A1-1*: Diagram of the Solar System and heliosphere showing the trajectories of the unmanned space probes Pioneer 10, Pioneer 11, Voyager 1 and Voyager 2. These probes were the first to study the outer Solar System, taking advantage of a rare alignment of the gas giant planets to visit them all. (Credit NASA, http link to image (http://pixabay.com/en/solar-system-space-bow-shock-11578/; see also http://www.nasa.gov/centers/ames/news/releases/2001/01images/Pioneer10/pioneer10.html (image link), Public Domain, https://commons.wikimedia.org/w/index.php?curid=38037924))*

The in-situ magnetospheric exploration of the four large planets of our solar system had started with Pioneer 10's flyby of Jupiter in Dec. 1973. The second collection of field, particle and radio data of the gas giant was carried out by Pioneer 11 in Dec. 1974, before this spacecraft made its closest approach to Saturn in Sep. 1979. Around the same period, Voyager 1 (2) flew by Jupiter in Mar. (Jul.) 1979 then Saturn in Nov. (Aug.) 1980 (1981). As of today, only Voyager 2 visited the magnetospheres of Uranus (Jan. 1986) and Neptune (Aug. 1989). Galileo had remained the only spacecraft to orbit an outer planet for several years (1995 - 2003) until the arrival of Juno at Jupiter in 2016. Between 2004 and 2017, the Cassini mission had provided a wealth of in-situ data pertinent to the study of magnetospheric particles at Saturn.

In this paper, we present our current understanding of the processes that shape the spatial distributions of energetic electrons trapped in the magnetospheres of Jupiter ($L < 6$), Saturn ($L < 15$) and Uranus ($L < 15$) obtained by combining multi-instrument analyses of data from past missions (Pioneer, Voyager, Galileo, Cassini) and computational models of charged particle fluxes. To determine what controls the energy and spatial distributions throughout the different magnetospheres, we compute the time evolution of particle distributions with the help of a diffusion theory particle transport code that solves the governing 3-D Fokker-Planck equation. Particle, field and wave datasets are either used to provide model constraints, assist in modeling physical processes, or validate our simulation results.

We first emphasize our latest results regarding the relative (or coupled) role of mechanisms at Saturn, including the radial transport and interactions of electrons with Saturn's dust/neutral/plasma environments and waves, as well as particle sources from high-latitudes, interchange injections, and outer magnetospheric region.

The lessons learned from our modeling of electron distributions at Saturn are used to identify the processes that may be missing in our modeling of Jupiter's energetic electron environment or those in need to be implemented using new modeling concepts.

Our first physics-based modeling of electron populations at Uranus is also assessed with our data-model comparison approach.

B. DATA SETS & MODELING APPROACH

B1. DATASETS

We primarily use particle, field and wave data from Pionner 10 & 11 (e.g., Divine&Garrett1983), Voyager 2 (e.g., Divine&Garrett1983), Galileo Probe (Fischer1996, Mihalov1998), and Cassini (Young2004, Krimigis2004, Dougherty2004, Gurnett2004). Particle and field data are used to both constrain physics-based models at their boundary conditions, model internal particle sources and discuss simulation results with in-situ observations.

Instrument	Data Type	References
	Pioneers 10 and 11	
Helium vector magnetometer (HVM)	vector magnetic field	*Smith et al.* [1976]
Flux gate magnetometer (FGM)	vector magnetic field	*Acuna and Ness* [1976*a*, *b*]
Plasma analyzer (PA)	electrons and protons, 0.1 to 4.8 keV	*Frank et al.* [1976]
Geiger tube telescope (GTT)	electrons >0.06, 0.55, 5, 21, 31 MeV protons 0.61–3.41 MeV	*Van Allen et al.* [1974, 1975], *Van Allen* [1976], and *Baker and Van Allen* [1977]
Trapped radiation detector (TRD)	electrons >0.16, 0.26, 0.46, 5, 8, 12, 35 MeV protons >80 MeV	*Fillius and McIlwain* [1974], *Fillius et al.* [1975], and *Fillius* [1976]
Low-energy telescope (LET)	protons 1.2–2.15 and 14.8–21.2 MeV	*Trainor et al.* [1974, 1975] and *McDonald and Trainor* [1976]
Electron current detector (ECD)	electrons >3.4 MeV	*Simpson et al.* [1974, 1975]
Fission cell (F1)	protons >35 MeV	*Simpson and McKibben* [1976]
	Voyagers 1 and 2	
Flux gate magnetometer (MAG)	vector magnetic field	*Ness et al.* [1979*a*, *b*]
Planetary radio astronomy (PRA)	electric vector, 1.2 kHz to 40.5 MHz	*Warwick et al.* [1979*a*, *b*] and *Birmingham et al.* [1981]
Plasma wave (PWS)	10 Hz to 56 kHz	*Scarf et al.* [1979] and *Gurnett et al.* [1979]
Plasma science (PLS)	electrons 10–6000 eV ions 10–6000 V	*Bridge et al.* [1979*a*, *b*], *Bagenal and Sullivan* [1981], and *Scudder et al.* [1981]
Low-energy charged particle (LECP)	electrons >15 keV ions >30 keV	*Krimigis et al.* [1979*a*, *b*, 1981]
Cosmic ray telescope (CRT)	electrons 3–110 MeV ions 1–500 MeV/nucleon	*Vogt et al.* [1979*a*, *b*]
	Earth	
Radio telescopes	UHF intensity and polarization	*Berge and Gulkis* [1976] and *dePater and Dames* [1979]

Table A1-1*: Overview of key Pioneer 10&11 and Voyager 1&2 datasets used for our models (*Divine&Garrett1983*).*

Channel	Energy ranges (MeV nucleon^{-1}) for particle species				
	e^-	p^+	He	C	S
E1	3.2	42	42	75	125
E2	8	62	62	110	210
E3	8	62	62	110	210
P1	66	42–131	42	75	125
P2	100	62–131	62	110	210
P3	203	62–92	62–530	110	210
He	450	–	62–136	110	210
HV	–	–	–	110–168	210

Table A1-2*: Galieo Probe EPI datasets (*Fischer1996*).*

ELS	Species	Channel Nbr.	Total Energy Band (keV)	
	Electrons	63	0.58 10^{-3} - 26.04	
LEMMS	**Species**	**Channel**	**Energy (keV)**	**Mean Energy (keV)**
	Electrons	C0	18-40	26.8
	Electrons	C1	27-48	36.0
	Electrons	C2	41-60	45.6
	Electrons	C3	56-100	74.8
	Electrons	C4	92-183	129.8
	Electrons	C5	175-300	229.1
	Electrons	C6	265-550	281.8
	Electrons	C7	510-832	651.4

Table A1-3*: Overview of Cassini CAPS/ELS and MIMI/LEMMS particle datasets used for our models (*Young2004, Krimigis2004*).*

B2. MODELING APPROACH

We model the energy and spatial distributions of electrons in the different magnetospheres with the help of a diffusion theory particle transport code that solves the governing three-dimensional Fokker-Planck equation (SantosCosta2003, SantosCosta&Bolton2008). This numerical code, referred to hereafter as *DSC*'s diffusion transport code, computes the time evolution of particle distributions in a phase space that depends on energy, latitude, and radial distance. In our theoretical approach, the angular parameter is characterized by the pitch-angle variable. The radial distance is defined by the L parameter (e.g. Roederer1970, Schulz&Lanzerotti1974). The particle gyro-phase is assumed uniform in our treatment. Eq.(1) is the diffusion transport equation we numerically solve to calculate the electron distributions:

$$\begin{aligned}\frac{\partial f(J_1,J_2,J_3,t)}{\partial t} &= (S)+(L)+\frac{1}{G}\frac{\partial}{\partial L}\left[GD_{LL}\frac{\partial f(M,J,L,t)}{\partial L}\right]_{M,J} \\ &- \frac{1}{G'}\sum_{i=1,2}\frac{\partial}{\partial Q_i}\left[G'\left(\frac{dQ_i}{dt}\right)f(E,y,L,t)\right] \\ &+ \frac{1}{G'}\sum_{i,j=1,2}\frac{\partial}{\partial Q_i}\left[G'D_{ij}\frac{\partial f(E,y,L,t)}{\partial Q_j}\right] \qquad (1)\end{aligned}$$

where f is the particle phase space distribution function averaged over the magnetic drift shells. $(J_i)_{i=1,3}$ are the adiabatic invariants associated with the elementary motions of charged trapped particles (Northrop1963). M (=$J_1 q/m_0$ with q the elementary charge & m_0 the electron rest mass) is the relativistic magnetic moment & J (=J_2) the second invariant (e.g., Schultz&Lanzerotti1974). E (=Q_1) is the kinetic energy and y (=Q_2) the sine of equatorial pitch-angle α_{eq}. $(D_{ij})_{i,j=1,2}$ and $(dQi/d\,t)_{i=1,2}$ are diffusive and friction terms, respectively. (S) = $\sum f/\tau_s$ are source terms and (L) = $-\sum f/\tau_l$ loss terms. D_{LL} is the so-called radial diffusion coefficient term.

Various phase spaces are numerically coupled to solve Eq.(1): the (M, J, L) action variable phase space allows to simulate the cross drift shell motion of trapped particle populations (i.e. radial transport), while the (E, y, L) phase space only accounts for processes unrelated to radial transport (e.g. SantosCosta2003, SantosCosta&Bolton2008). To make the change of variables and numerically switch between phase spaces, two Jacobian determinants are computed (Schulz&Lanzerotti1974):

$$\begin{aligned}G &= \frac{\partial(J_1,J_2,J_3)}{\partial(M,J,L)} \\ &= \det\begin{vmatrix}\frac{\partial J_1}{\partial M} & \frac{\partial J_2}{\partial M} & \frac{\partial J_3}{\partial M}\\ \frac{\partial J_1}{\partial J} & \frac{\partial J_2}{\partial J} & \frac{\partial J_3}{\partial J}\\ \frac{\partial J_1}{\partial L} & \frac{\partial J_2}{\partial L} & \frac{\partial J_3}{\partial L}\end{vmatrix}\end{aligned}$$

$$\begin{aligned}G' &= \frac{\partial(J_1,J_2,J_3)}{\partial(Q_1,Q_2,L)} \\ &= \det\begin{vmatrix}\frac{\partial J_1}{\partial E} & \frac{\partial J_2}{\partial E} & \frac{\partial J_3}{\partial E}\\ \frac{\partial J_1}{\partial y} & \frac{\partial J_2}{\partial y} & \frac{\partial J_3}{\partial y}\\ \frac{\partial J_1}{\partial L} & \frac{\partial J_2}{\partial L} & \frac{\partial J_3}{\partial L}\end{vmatrix}\end{aligned}$$

Figure B-1 presents a schematic view of the physical processes and control parameters we would eventually have to consider regarding the modeling of energetic electrons at Jupiter, Saturn and Uranus. Sections C, D and E emphasize the processes currently accounted for in our physical model for each of the magnetospheres. We limit our modeling of energetic electron populations to the 1 - 5 L region at Jupiter, and up to L = 15 for Saturn (R_S) and Uranus (R_U).

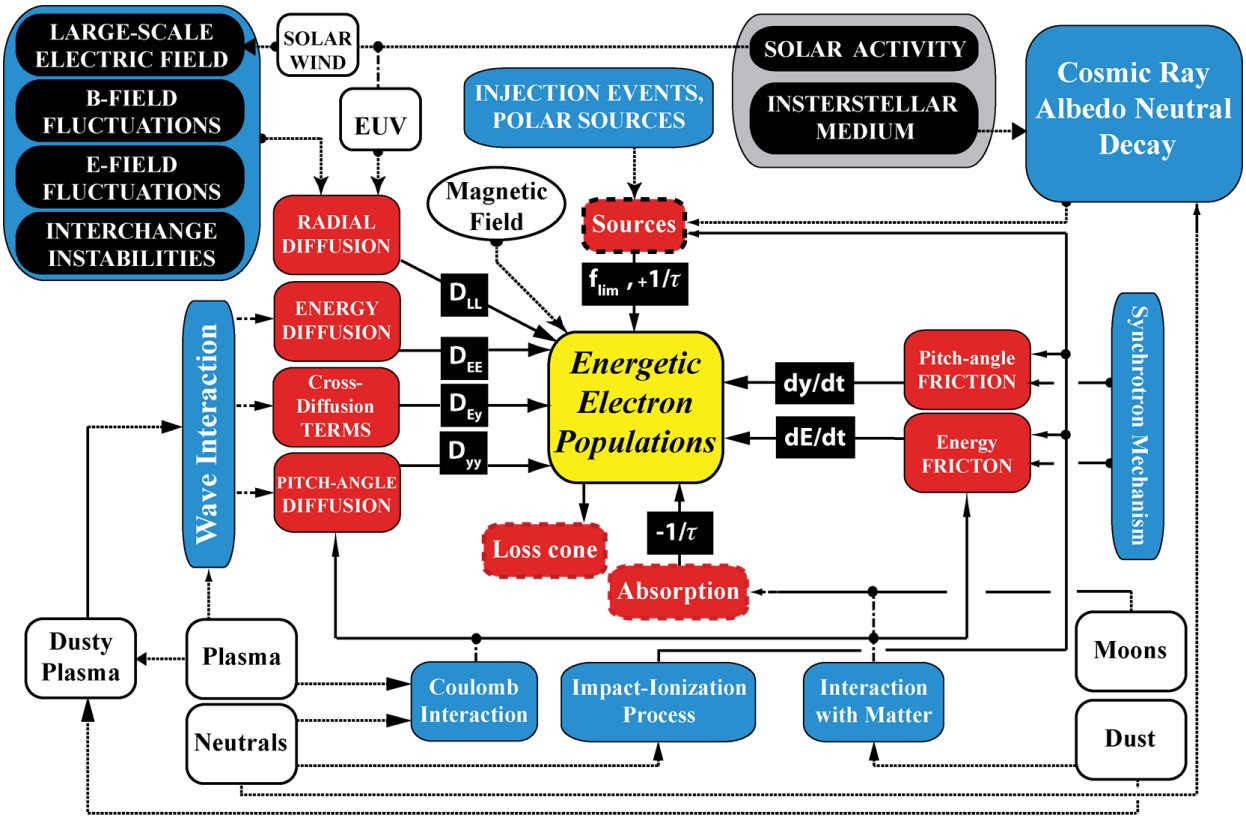

***Figure B1-1**: Theoretical approach for our three-dimensional modeling of electron populations at outer planets.*

When accounting for the processes highlighted in Fig. B-1 and after rearranging the different terms, Eq. (1) takes the form:

$$
\begin{aligned}
\frac{\partial f}{\partial t} &= \sum \frac{f}{\tau_s} - \sum \frac{f}{\tau_l} \\
&+ \left[\frac{1}{G}\frac{\partial G}{\partial L} D_{LL} + \frac{\partial D_{LL}}{\partial L}\right] \frac{\partial f^{\times}}{\partial L} + (D_{LL}) \frac{\partial^2 f^{\times}}{\partial L^2} \\
&- \left[\frac{1}{G'}\left(\frac{\partial G'}{\partial E}\right)\left(\sum \frac{dE}{dt}\right) + \sum \frac{\partial}{\partial E}\left(\frac{dE}{dt}\right)\right] f^{*} \\
&- \left[\frac{1}{G'}\left(\frac{\partial G'}{\partial y}\right)\left(\frac{dy}{dt}\right) + \frac{\partial}{\partial y}\left(\frac{dy}{dt}\right)\right] f^{*} \\
&- \left[\left(\sum \frac{dE}{dt}\right) - \frac{1}{G'}\left(\frac{\partial G'}{\partial E}\right) D_{EE} - \frac{\partial D_{EE}}{\partial E} - \frac{1}{G'}\left(\frac{\partial G'}{\partial y}\right) D_{yE} - \frac{\partial D_{yE}}{\partial y}\right] \frac{\partial f^{*}}{\partial E} \\
&- \left[\left(\frac{dy}{dt}\right) - \frac{1}{G'}\left(\frac{\partial G'}{\partial E}\right) D_{Ey} - \frac{\partial D_{Ey}}{\partial E} - \frac{1}{G'}\left(\frac{\partial G'}{\partial y}\right)\left(\sum D_{yy}\right) - \sum \frac{\partial D_{yy}}{\partial y}\right] \frac{\partial f^{*}}{\partial y} \\
&+ (D_{EE}) \frac{\partial^2 f^{*}}{\partial E^2} + 2\,(D_{yE}) \frac{\partial^2 f^{*}}{\partial E \partial y} + \left(\sum D_{yy}\right) \frac{\partial^2 f^{*}}{\partial y^2}
\end{aligned}
\qquad (2)
$$

In Eq.(2), $f = f(J_1,J_2,J_3,t)$, $f^x = f(M,J,L,t)$ and $f^* = f(E,y,L,t)$. The latter notations mean that $f \equiv f^x \equiv f^*$ with $M = g_1(J_1,J_2,J_3)$, $J = g_2(J_1,J_2,J_3)$, $L = g_3(J_1,J_2,J_3)$, $E = g_4(J_1,J_2,J_3)$, $y = g_5(J_1,J_2,J_3)$ and $(g_i)_{i=1,5}$ functions of J_1, J_2 and J_3. The first and second-order derivatives are numerically computed with either central, forward or backward differences using Taylor series approximations. The different schemes are set by the origin of the diffusive and friction terms in the transport equation.

C. MODELING SATURN'S ENERGETIC ELECTRON ENVIRONMENT

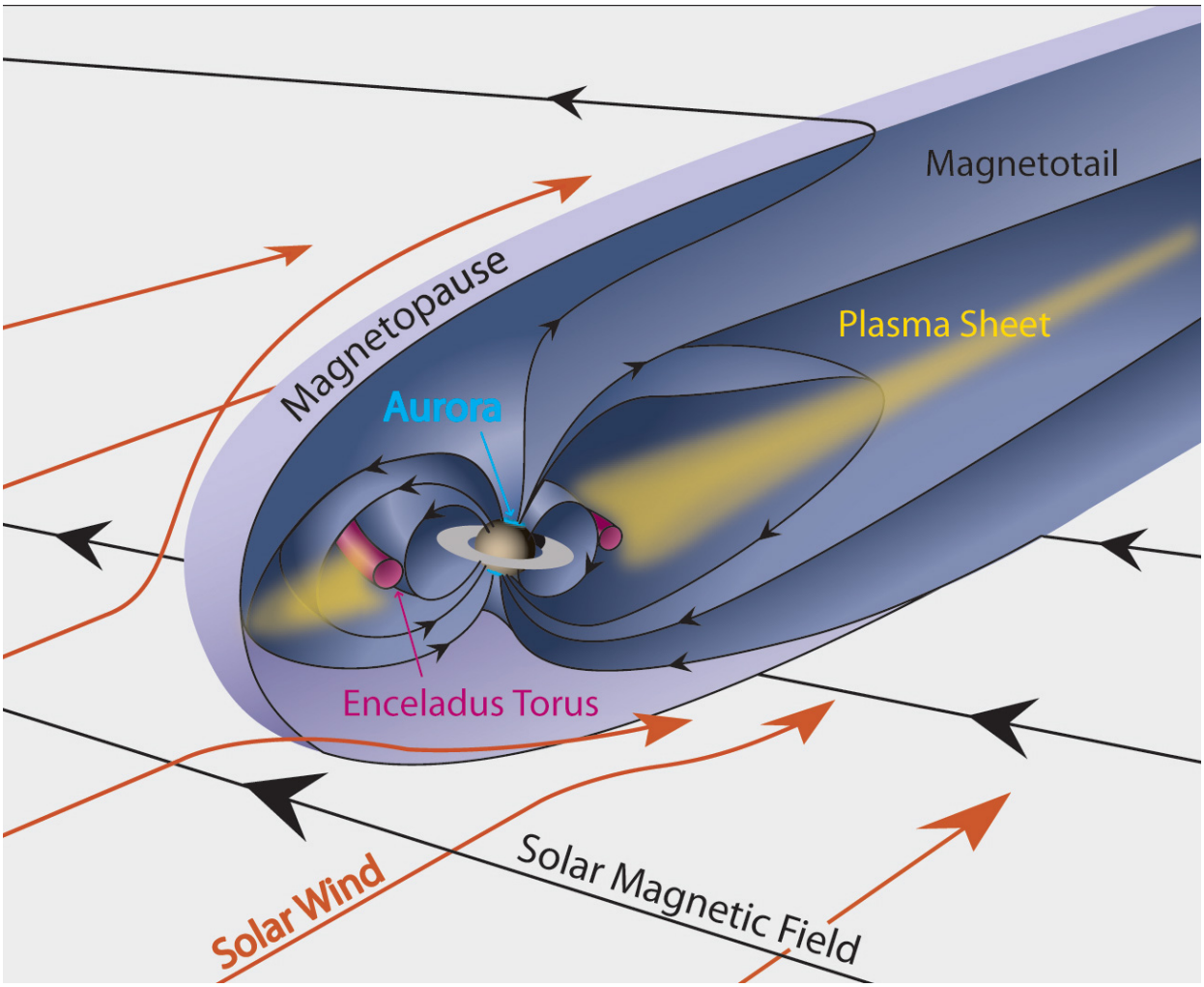

Figure C1-1*: Schematic view of Saturn's magnetosphere. (See Bagenal, Nature 433, 695-696, 2005.) Credit: Fran Bagenal & Steve Bartlett (https link to image (https://lasp.colorado.edu/home/mop/files/2012/04/Saturn3D_15.jpg)).*

C1. MAGNETIC FIELD MODEL

The encounters of Pioneer and Voyager spacecraft with Saturn in the late 1970's and early 1980's had shown that Saturn is surrounded by a system of different currents (Davis1990, Connerney1983). Beyond ~15 R_S, the magnetic field's features and Saturn's magnetosphere boundaries were observed to be controlled by magnetopause and tail currents systems (e.g., Khurana2006, Arridge2008, Achilleos2010). Closer to the planet, the topology of Saturn's magnetic field departs from a dipolar configuration beyond ~4-6 R_S. Field lines are moderately, but measurably stretched out in the equatorial plane, due to the presence of equatorial ring currents (e.g., Connerney1982, Connerney1984).

The lack of agreement between magnetic measurements at different periods had forced models of the Saturnian disk current to account for the condition of the magnetosphere. For instance, the ring current parameters have to vary according to Saturn's magnetosphere size (e.g., Bunce2007). Within ~18 R_S, it was later confirmed that the field departs from a dipole and become a smoothly-warped magnetodisk, with the warping increasing with radial distance (e.g., Arridge2008, Carbary2010).

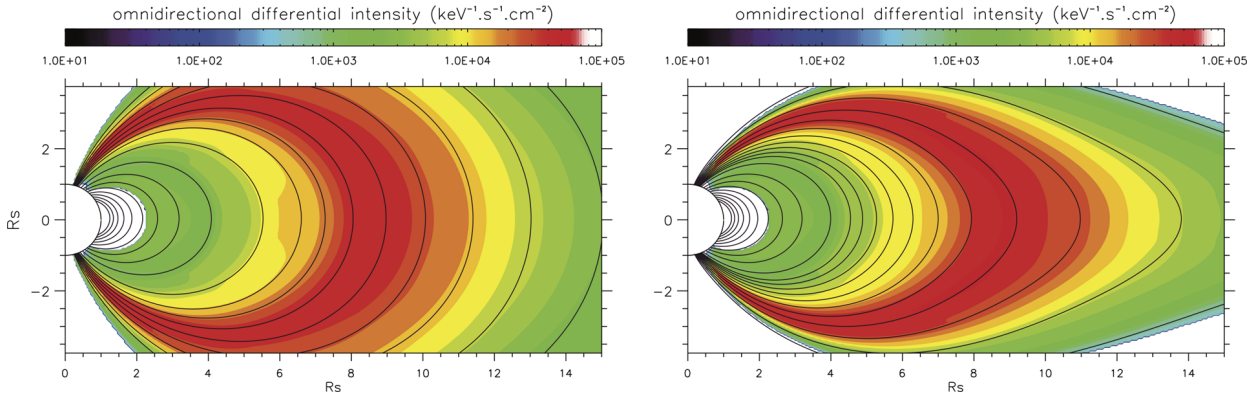

***Figure C1-2**: Meridian distributions of 18-40 keV-energy electrons (left: dipole field model; right: magnetospheric field model (Khurana2006)). MIMI-LEMMS C0 data were averaged over the period 2004-2013. For each magnetic configuration, only particles trapped along field lines that map onto the equator inside L = 20 are displayed. The subtile discrepancies in the spatial distributions justify the use of a magnetospheric magnetic field model instead of a dipolar configuration, although the conclusions we here draw from a physics-based modeling of mechanisms that shape mission-averaged particle distributions are unlikely influenced by the magnetic field configuration.*

For the present modeling work, a non-dipolar magnetospheric field model was implemented in our data processing and modeling tools (Fig. C1-2) to refine the description of radial and angular profiles of warm to energetic electrons when using all Cassini data available for the ~2-15 L region and period 2004-2013 (Fig. C1-3). However, we've opted for an axisymmetric magnetospheric model to facilitate the description then the numerical computation of Cassini observations of particle distributions (Khurana2006, Khurana2009).

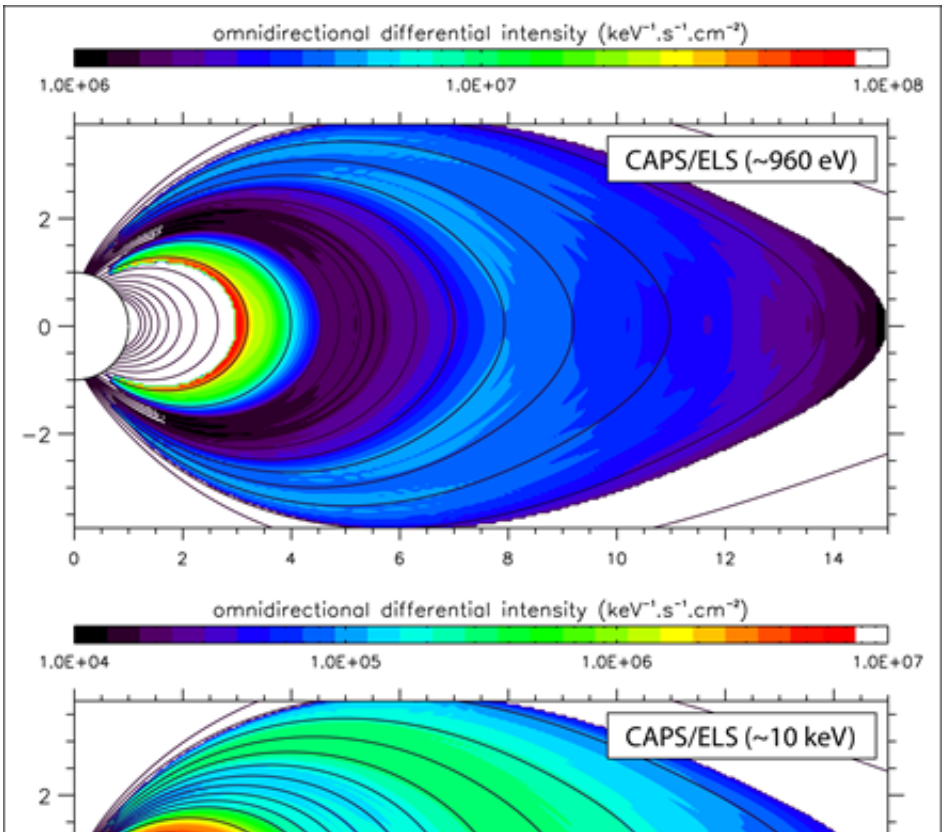

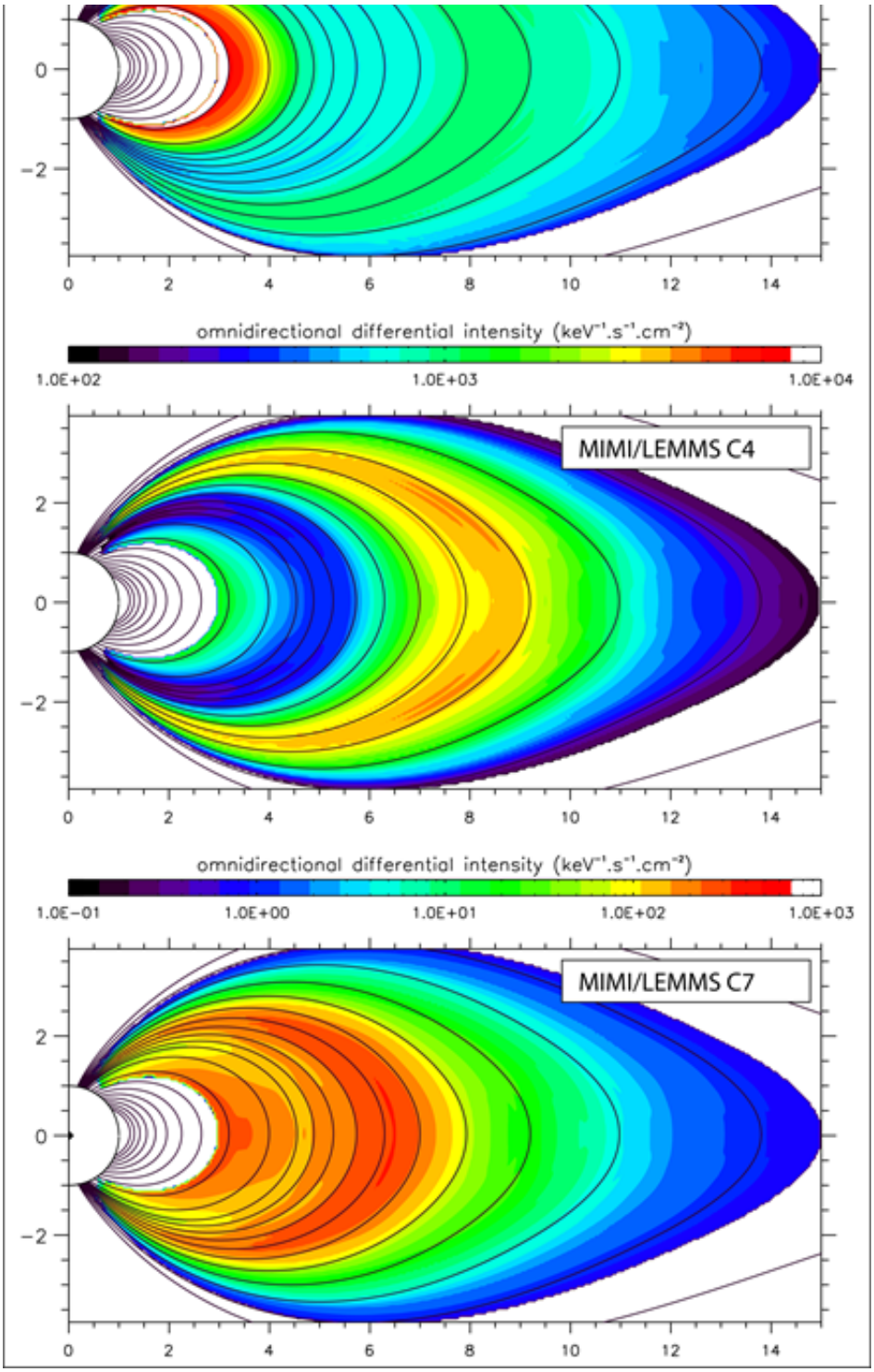

Figure C1-3*: Samples of mission-averaged data for different energy channels of Cassini CAPS-ELS and MIMI-LEMMS instruments. Data were averaged over the period 2004-2013, when both instruments were operating. CAPS/ELS was turned off for good in 2013.*

C2. MOTIVATION FOR PHYSICS-BASED DEVELOPMENT

Few physical models have been used in the past to investigate the distribution and dynamical behavior of Saturn's energetic electron populations over a large region of Saturn's magnetosphere. Two physics-based models were first developed to examine the role of inward transport, moons, dust and neutral environments, and waves in the distribution of electrons with energies of hundreds of keV to tens of MeV at L = 1-6 (SantosCosta2003, Lorenzato2012). Results from a physical modeling approach confirmed strong electron absorption rates within the densest parts of the Saturnian ring system, resulting in drastic drops in electron flux inside L ~2.3. Moons cause local absorptions, which are observed in-situ by sharp and narrow depletions (or micro-signatures) in electron intensities (e.g., Roussos2007). Model results also suggested that neutrals play an important role in the spatial distribution of electrons beyond L ~2.3, in contrast to dust particles which likely only contribute to the energy and radial profiles of near-equatorial electrons (SantosCosta2003, Lorenzato2012).

Gyro resonant interactions between electrons and Whistler mode Chorus waves were modeled to evaluate the energization mechanisms for electrons by these waves and discuss the origin of the Kronian radiation belt. Model results of wave-particle interactions at Saturn first remained inconclusive beyond L~4-5 (Lorenzato2012, Shprits2012). Recently, the formation of Saturn's MeV electron belts inside L ~4 was linked to particle energization by Z-mode waves (Woodfield2018). Woodfield2019 argued that Whistler mode Chorus waves may be more effective in energizing electrons than previously thought. Woodfield2020 discuss the effect of hiss waves on the energy of the electrons in the radiation belts and find that such waves strongly accelerate electrons. Due to the high latitude location of the hiss, this acceleration is confined to mid to low pitch angles and leads to butterfly pitch angle distributions. Based on Cassini survey results of wave global distributions at Saturn (e.g., Menietti2014, Menietti2015), Yu2019 examined the combined effects of near equatorial Whistler mode Chorus waves and high-latitude Z-mode waves at a radial distance of 6 R_S. They found that these two types of waves at different latitudes can jointly control the fluxes of Saturn's radiation belt electrons right inside Dione's orbit (6.2 R_S). As pointed out in Yu2019, the analyses of combined diffusion of electrons by these waves and/or other plasma waves within larger magnetospheric regions remain to be carried out to fully confirm the effectiveness of particle energization from coupled wave interactions at Saturn.

Finally, preliminary comparison results between Cassini particle data and a computational model for the region L = 2-15 (Clark2014) have highlighted the role of neutrals and radial transport in the angular and radial distributions of energetic electrons at Saturn. Clark2014 pointed out that discrepancies exist in the simulated evolution of the PAD and that field-aligned electron fluxes were grossly underestimated. They postulated these differences were due to an incomplete physical picture and suggested further mechanisms be incorporated into the model.

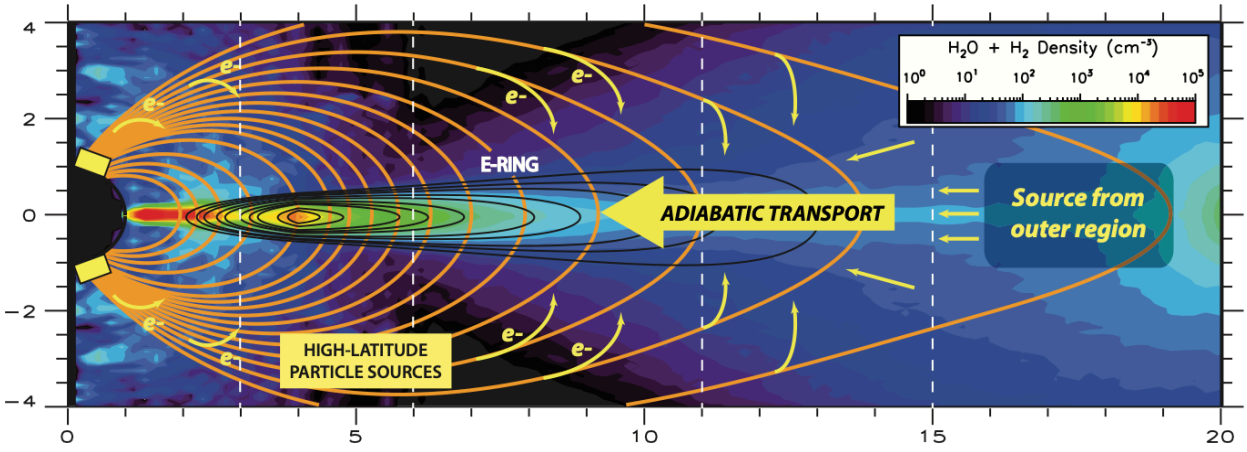

Figure C1-4*: Composite image highlighting the regions where Cassini instruments observed persistent angular features (PADs): PADs of warm to energetic electrons evolve from near isotropic distributions at L >~ 15 to field-aligned at L ~11-15, before gradually becoming butterfly at L ~6-11 and finally pancake or quasi-isotropic at L ~< 6-8. It is believed that the radial transport & interactions of electrons with neutrals, dust particles (e.g., E-ring), cold plasma, EM waves & the presence of particle sources at high-latitudes, outer region & from particle injections contribute to the radial, energy, and angular distributions of warm to energetic electrons (Clark2014). Here we re-examine the individual and combined roles of radial transport and different types of interactions and particle sources.*

In the present work, we thus re-examine the distributions of ~1 keV to ~1 MeV-energy electrons that are subject to adiabatic transport, collision with Saturn's neutrals, dust materials and cold plasma populations and resonance with waves at L < 15 (Fig. C1-4). We reappraise the work of SantosCosta2003 for a larger magnetospheric region, while pursuing the work of Clark2014 in order to further investigate the origin(s) and radial evolution of electrons' Pitch Angle Distributions (PADs) at Saturn using a data-model comparison approach.

C3. PHYSICS-BASED MODEL RESULTS

We here focus on characterizing radial transport mechanisms and interaction of energetic electrons with neutrals, dust & cold plasma particles and plasma waves:

- The radial transport is constrained by MIMI/LEMMS observations of micro-signatures (Roussos2007) and assumed to be adiabatic (Kollmann2018). See Fig. C1-5.

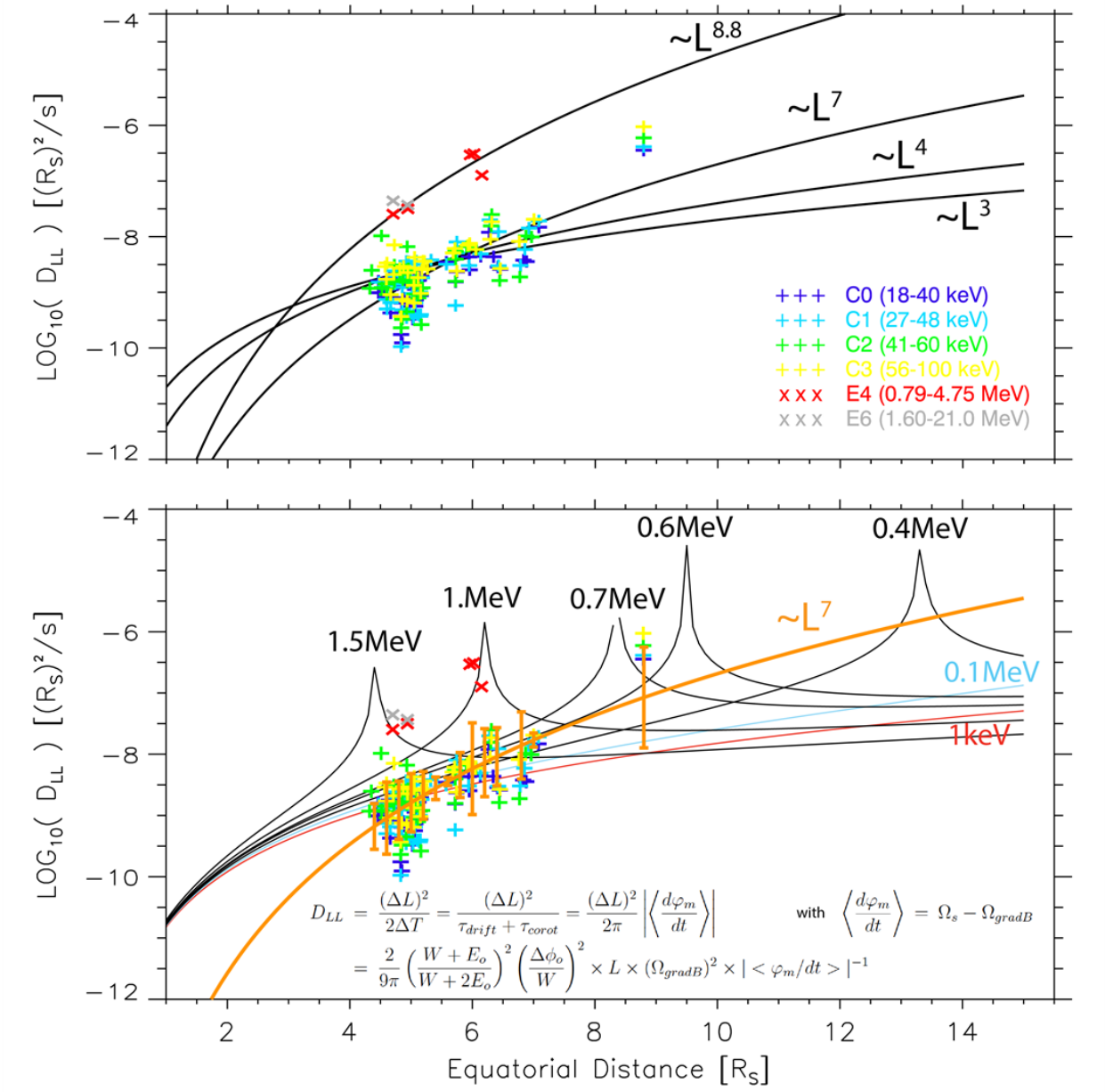

Figure C1-5: *Radial diffusion coefficients tested in our model. Radial transport is either driven by centrifugal interchange, electric or magnetic perturbations, or diurnal atmospheric winds. These coefficients account or not for energy and pitch-angle dependence. + and x-symbols correspond to radial diffusion coeffiecients derived from absorption micro-signatures of Tethys (~3.9 R_S) and Rhea (~8.7 R_S) moons (Roussos2007).The solid orange line is the linear fit to all data points in the [2;9] R_S range. The radial diffusion term for low-energy electrons resembles to the centrifugally driven diffusion coefficient (e.g., $D_{LL} = D_{\Omega}L^{3-4}$), while more energetic electrons could be driven by electric or magnetic perturbations (e.g., $D_{LL} = D_{em}L^{5-10}$). A unique expression of D_{LL} was determined to account for the observed energy and pitch-angle dependences.*

- The theoretical modeling of the interaction of electrons with neutrals, dust, cold plasma and waves require the computation of different terms for Eq.(1), as illsutrated with Figs. B1-1 and C1-6. We make use of different models of neutral environments (Tseng2011, Tseng2013), dust rings (SantosCosta2003, Horanyi2008, Kollmann2011, Lorenzato2012), and cold plasma (Clark2014, Lorenzato2012, Persoon2013, Persoon2020) and survey results of wave activity (Menietti2012, Menietti2015, Menietti2014) to carry out our modeling of particle interactions.

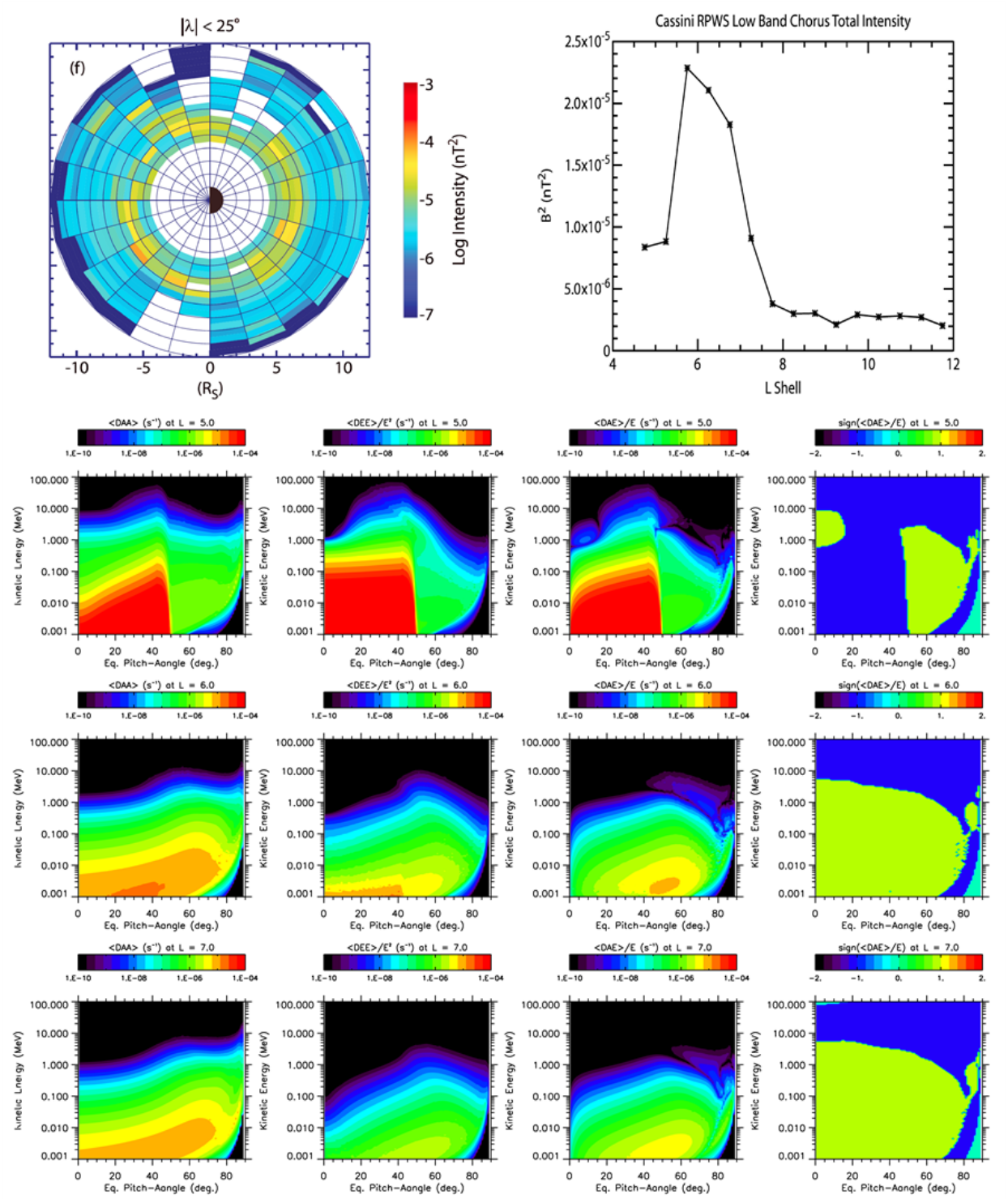

Figure C1-6*: Samples of whistler mode chorus waves coefficients (lower three panels; after Woodfield2019), calculated from the radial, longitudinal, and latitudinal distributions of spectral intensity (top left panel) and Chorus intensity averaged over all local times and latitudes (top right panel).*

- Different sources of warm to supra-thermal electrons at high-latitudes beyond ~10 R_S (after Clark2014, Clark2018) and from injection events inside ~10 R_S (after Paranicas2016) were constrained by Cassini CAPS/ELS & MIMI/LEMMS data

and implemented into our physical model to improve comparisons with in-situ data.

Figures C1-7, C1-8 and C1-9 display simulation results highlighting key coupled processes that contribute to the radial, energy and latitudinal distributions of energetic electrons at Saturn.

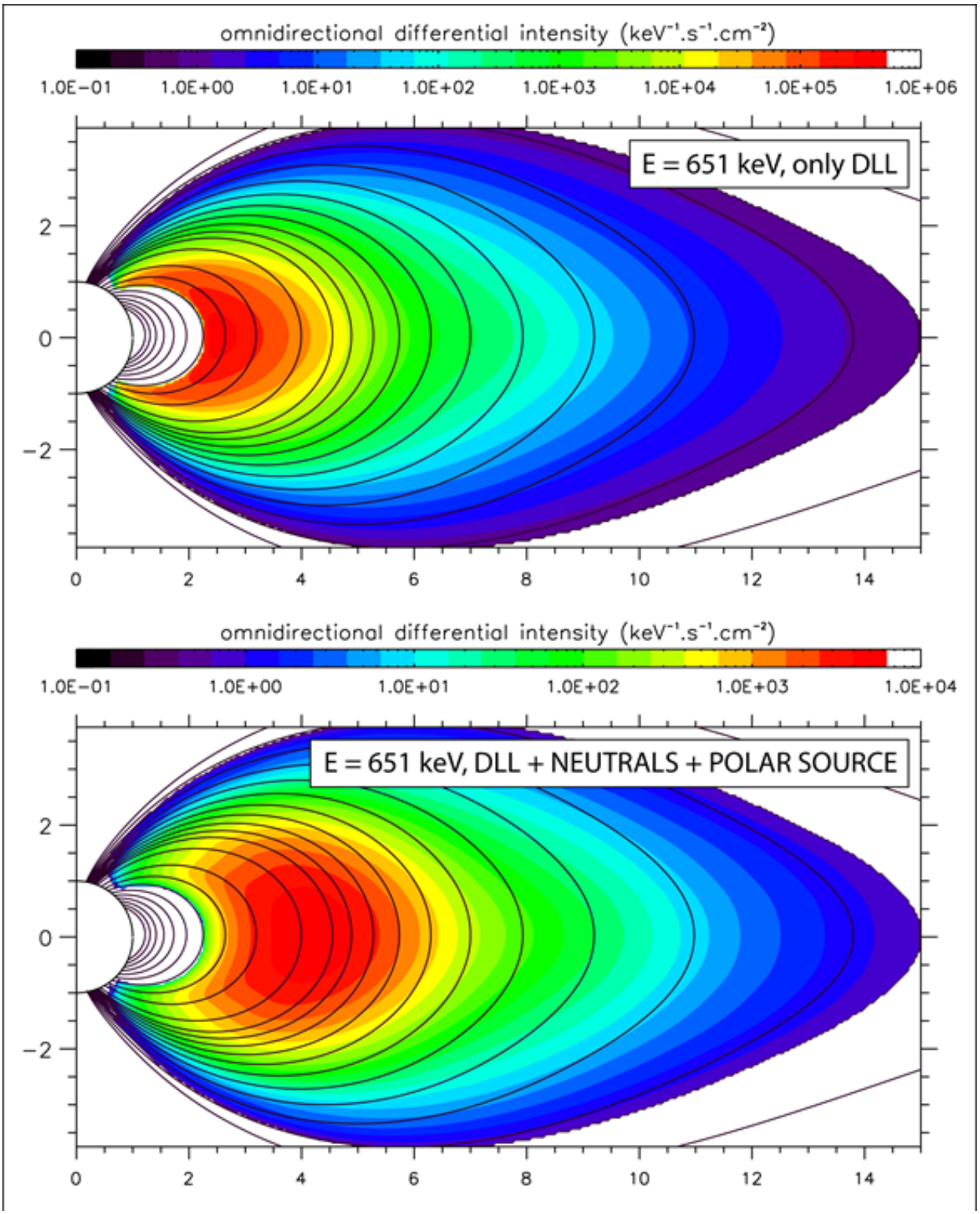

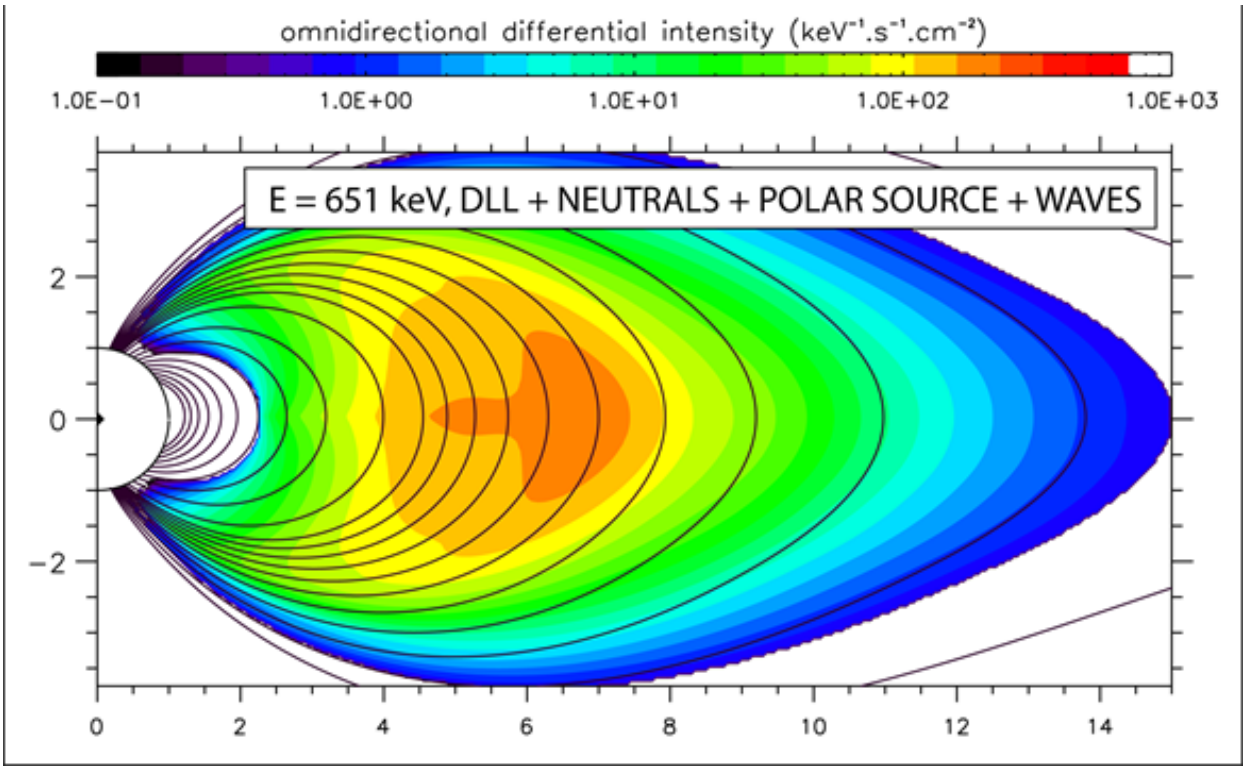

***Figure C1-7**: Simulated omni-directional differential intensity cartography of 650-keV energy electrons when model includes only radial transport (top 2d map), combines the diffusive radial transport with interaction with neutrals and a polar source of supra-thermal electrons (middle 2d map), and accounts for all previous processes plus interaction with whistler mode chorus waves (bottom 2d map).*

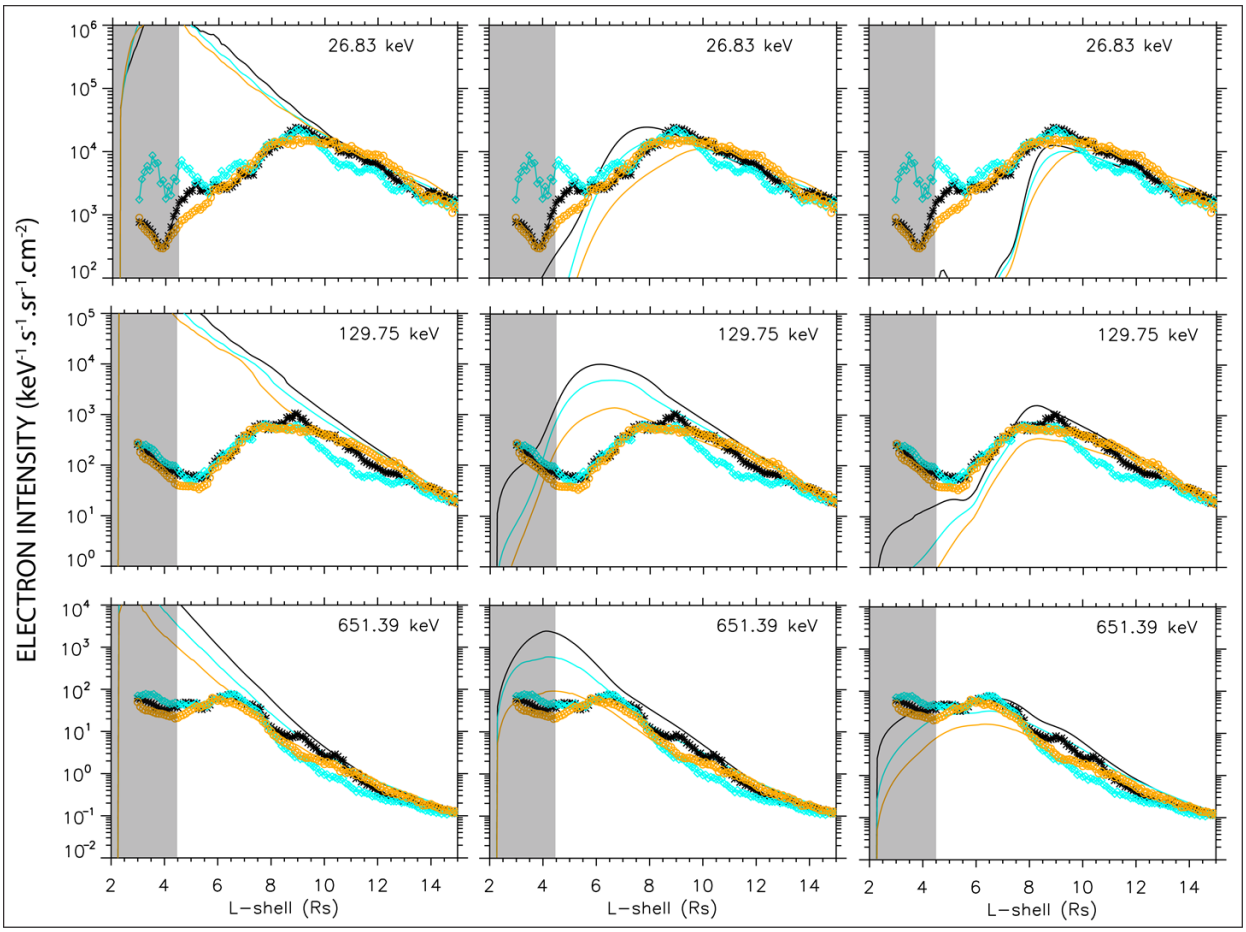

Figure C1-8: *Samples of comparisons between mission-averaged MIMI/LEMMS data and model when simulation includes only radial transport (left-hand panels), combines diffusive radial transport with interaction with neutrals and a polar source of supra-thermal electrons (middle panels), and accounts for all previous processes plus interaction with whistler mode chorus waves (right-hand panels). Circle, diamond and cross symbols are the data points. Simulations are plotted with solid lines. Black color is used to display radial profiles for 80^o, cyan for 40^o, and orange for 20^o pitch-angle. Gray boxes indicate where particle data are most likely contaminated by different background contamination sources (Schippers2008, Kollmann2011).*

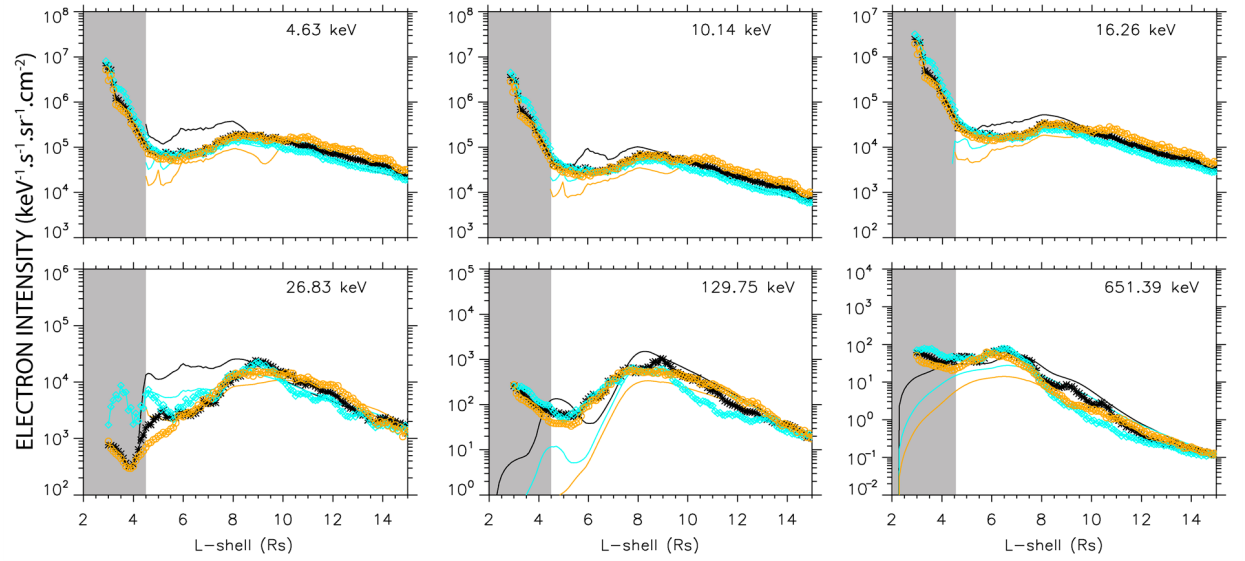

Figure C1-9: *Samples of comparisons between mission-averaged CAPS/ELS and MIMI/LEMMS data and model when simulation combines radial transport with interaction with neutrals, a polar source of supra-thermal electrons at high-latitudes at L >~ 10, interaction with whistler mode chorus waves at L ~< 10, and a source of 1-50 keV-energy electrons at L = 4-10. Circle, diamond and cross symbols are the data points. Simulations are plotted with solid lines. Black color is used to display radial profiles for 80º, cyan for 40º, and orange for 20º pitch-angle. Gray boxes indicate where particle data are most likely contaminated by different background contamination sources (Schippers2008, Kollmann2011).*

D. MODELING JUPITER'S ENERGETIC ELECTRON ENVIRONMENT

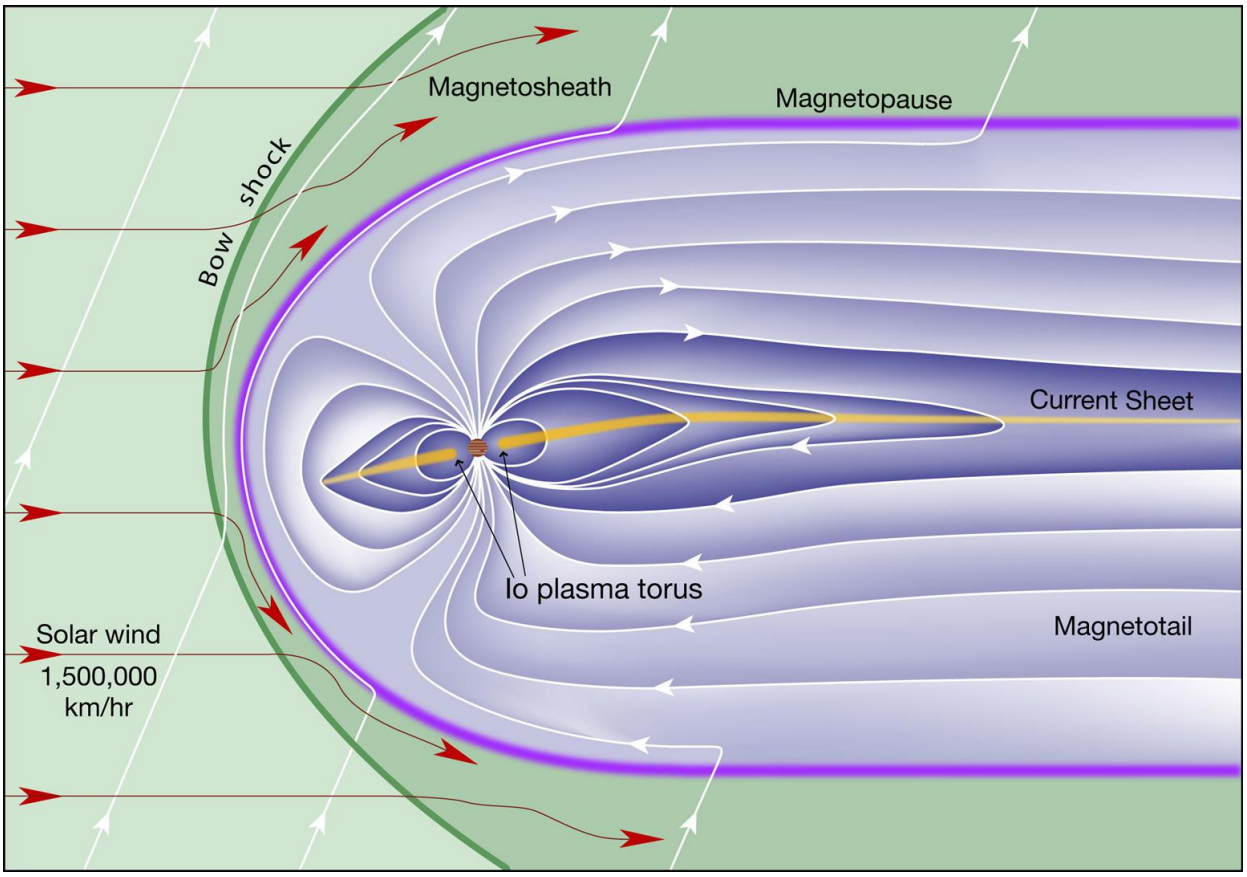

FIgure D1-1*: Schematic view of Jupiter's Magnetosphere. Credit: Fran Bagenal & Steve Bartlett (https link to image (https://lasp.colorado.edu/home/mop/files/2012/04/JupMag-8W.jpg)).*

D1. MAGNETIC FIELD MODEL

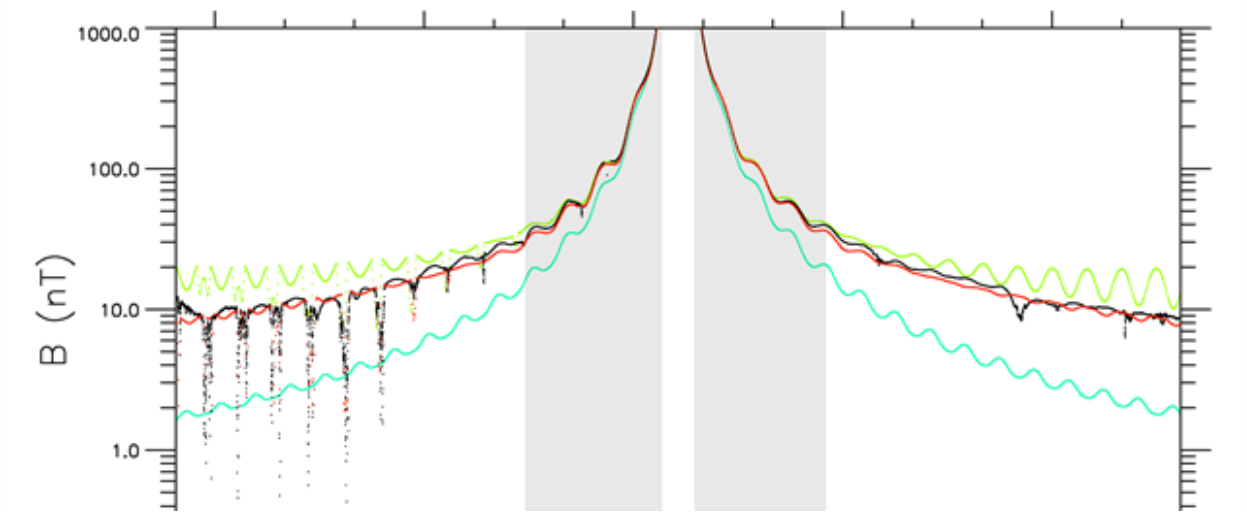

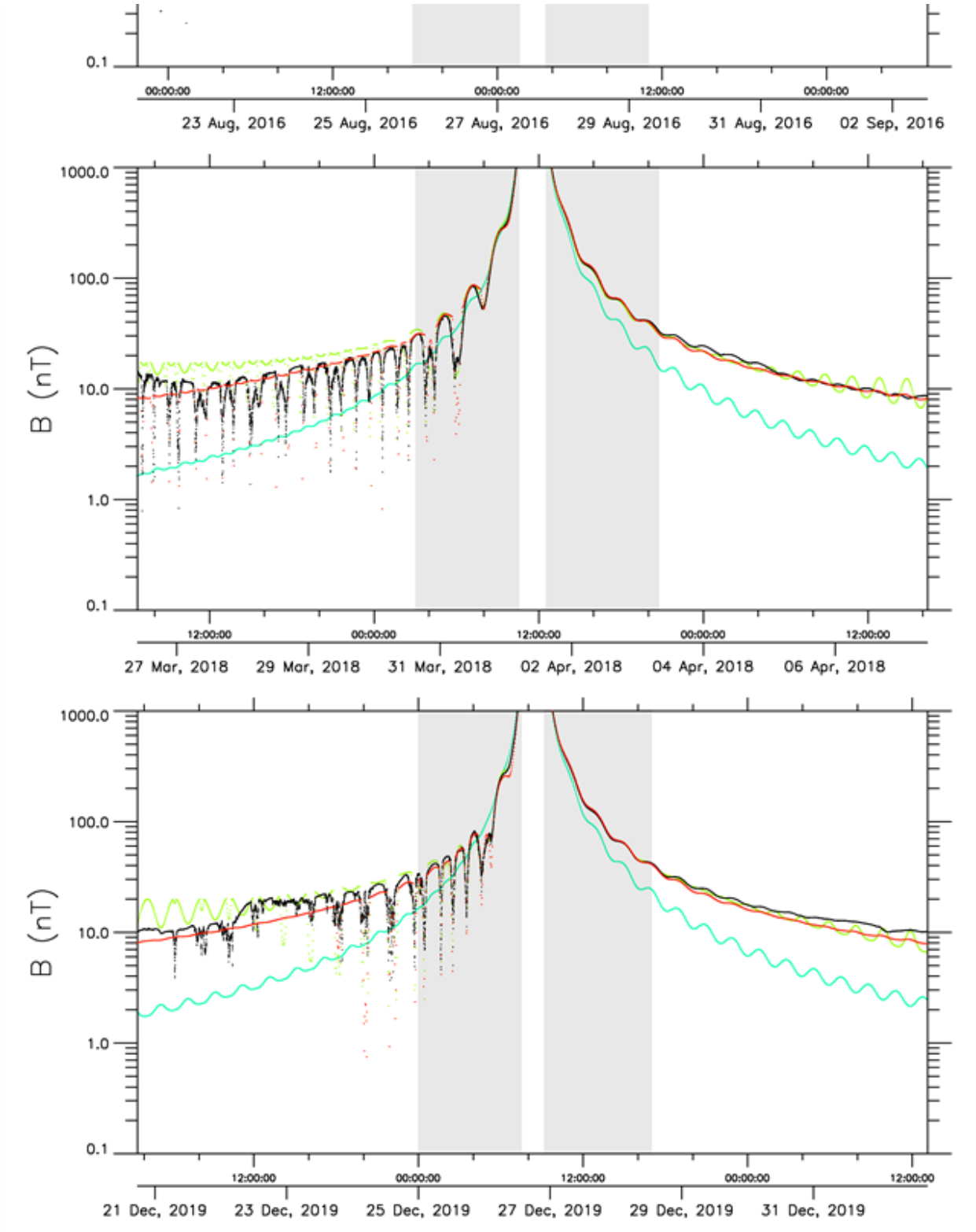

FIgure D1-2*: Comparisons between Juno MAG data (black) and magnetic field magnitude as predicted by JRM09 model (in magenta; Connerney2018), JRM09 + CAN2020 models (in green; Connerney2018, Connerney2020) and our magnetic field computation tool merging JRM09 + CAN2020 + Khurana's field models (in red; Connerney2018, Connerney2020, Khurana2005) along Juno trajctory for 10-12 days during orbits 1, 12 and 24. The gray zones define the periods when Juno is 7-30* R_J *from the planet.*

For the region 1-50 R_J, Jupiter's magnetospheric structure cannot be accurately represented with a simple field model such as an offset tilted dipole. Early radio and in-situ observations of Jupiter had suggested that the intrinsic field component of the giant planet possesses substantial quadrupole and octupole moments (e.g., Acuna1976, Acuna1983). Voyager 1 and 2's magnetic field measurements confirmed that the morphology of the magnetic field in the median Jovian magnetosphere is strongly influenced by the presence of a magneto-disc or current sheet (Connerney1981a,b). With the wealth of magnetic data from Galileo (1996-2003) and Juno (2016-current), early models of Jupiter's planetary field and median and outer magnetopheric regions have been improved with different levels of success (e.g., Connerney1981, Connerney1993, Khurana1992, Khurana1997, Khurana2005, Nichols2011, Nichols2015, Pensionerov2019). Figure D1-2 shows the capability and limitation of predicting magnetic field observations along Juno trajectory by different sets of published models.

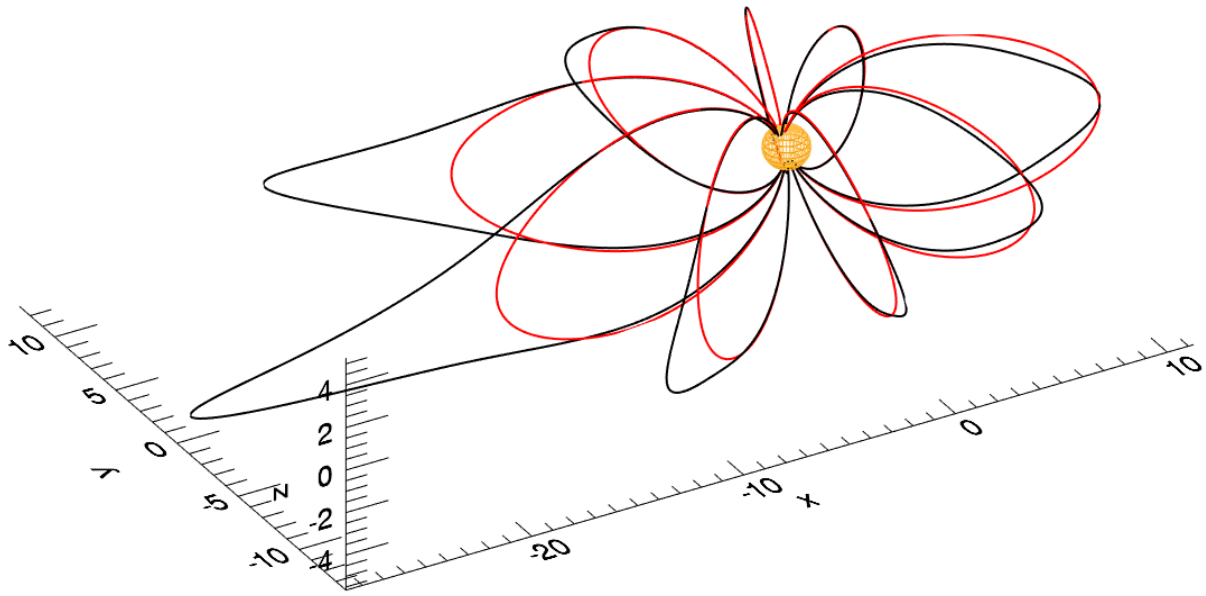

FIgure D1-3*: Reconstructed magnetic field lines that Juno crossed for 8 hours along its trajectory at intervals of 1 hour during orbit 21, starting at 7-20-2019UT16:00. Red field lines are traced using JRM09 + CAN2020 models, while the black ones are traced using our magnetic field computation tool.*

For the present work, we use a magnetic field computation tool that smoothly merges JRM09, CAN2020 and Khurana's field models (Connerney2018, Connerney2020, Khurana2005) to obtain the best fit possible with Juno and Galileo MAG data close to the planet (< 25-30 R_J) and at large radial distances. Figure D1-3 demonstrates how the choice of magnetic field model can lead to different interpretations of particle data when the magnetic field line tracing significantly departs from one model to the other.

D2. MOTIVATION FOR PHYSICS-BASED DEVELOPMENT

Until the arrival of Juno at Jupiter in 2016, little amount of in-situ particle data for the region 1-6 R_J was collected by Pioneer 10&11, Voyager 1, Galileo Probe and Orbiter (Fig. D1-4). Much of the research on the energetic and radiation-belt electron populations in that region had then been carried out with the help of Earth-based observations of Jupiter's synchrotron emission (e.g. dePater1981a,b, dePater1994, dePater1997, Levin2001, SantosCosta2001, Sicard2004, Garrett2005, SantosCosta&Bolton2008, Nenon2017).

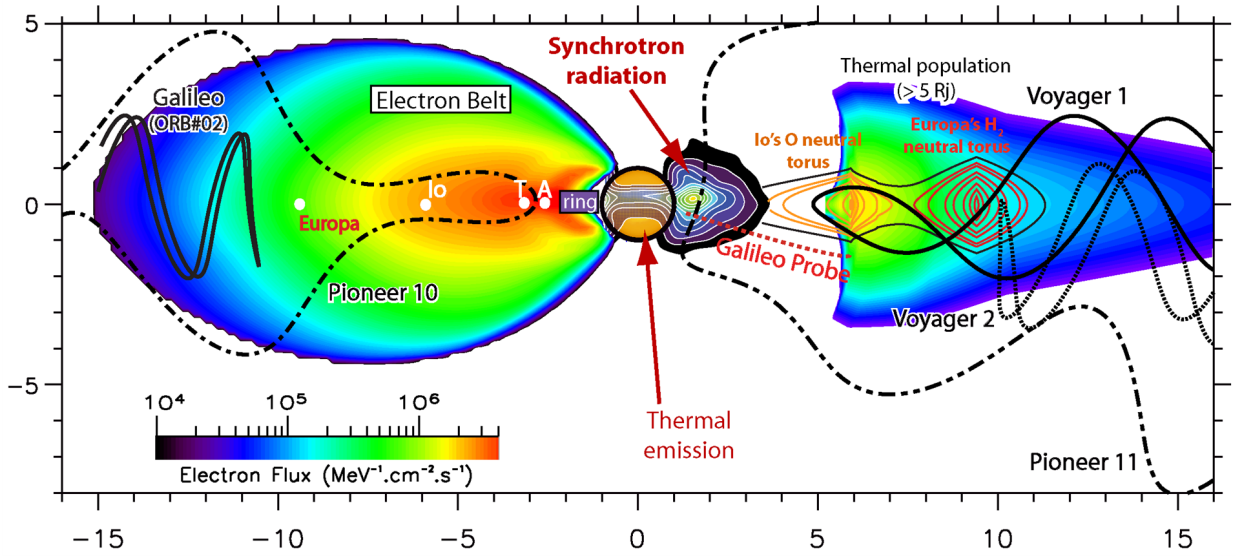

***FIgure D1-4**: Composite image of the spatial distributions of Jupiter's 10-MeV electron belt, thermal population, and microwave radiation (synchotron and non-thermal emissions). The location of a set of satellites, the main ring system and the spatial extension of Io's and Europa's main neutral torus are displayed. Overlapping are the trajectories of Pioneer 10-11, Voyager 1-2, Galileo probe and Galileo orbiter (orbit#2) in magnetic latitude and radial distance.*

Beyond the orbit of Io, the in-situ data returned by Pioneer's, Voyager's and Galileo's onboard instruments had provided the basis for the investigation of the extended energetic and radiation-belt electron environment. The first quantitative model of Jupiter's extended radiation zone, here and thereafter referred to as `the Divine model', was developed primarily based on particle data collected along Pioneer and Voyager flybys (Divine&Garrett1983). The model for the electrons was developed for the region inside 16 R_J. Although the Divine model is an empirical model, this latter is capable of matching the Pioneer energetic data remarkably well and to fit Galileo's with reasonable accuracy (Mihalov2000, Jun2003). For the region inside 3 R_J, modifications were yet made to the spatial and energy distributions to improve the comparisons between model outputs and radio measurements (Garrett2005). This was achieved with moderate success as Garrett2005's predictions of synchrotron emission are off by an order magnitude. Furthermore, Ezoe2010 argued that the Divine model is likely underestimating the ultra relativistic electron populations in the region 4-8 R_J by an order of magnitude. To improve Divine&Garrett1983's empirical model, particle data from the Galileo mission were incorporated into the Divine model to better constrain the electron distributions. The resulting and new model was referred to as GIRE, the Galileo Interim Radiation Environment (Garrett2003). Since, versions of GIRE were released to both improve and extend the Jovian radiation model up to 50 R_J (Garrett2012, deSoriaSantacruz2016, Jun2019). Despite the capability of calculating realistic electron fluxes near the equatorial and mid-latitude regions and beyond 3 R_J, the GIRE model does not tell us how the energetic electrons are produced, transported or lost within Jupiter's magnetosphere.

Combined with radio observations and in-situ measurements, the development of physics-based models of Jupiter's energetic and radiation-belt environments then offers a valuable method to examine the physical processes that maintain and govern the behavior of Jupiter's electron populations. Yet, few significant theoretical results were obtained that really address the key mechanisms of energization and transport in the middle magnetosphere (Shprits2012, Woodfield2014). The most recent advancement in the theoretical modeling of Jupiter's electron belt inside Europa's orbit had been presented by Nenon2017. To explain the Jovian electron belts morphology for the region ~6-9.5 R_J and the source of intense synchrotron radiation originating from the innermost radiation-belt region of the Jovian magnetosphere (~< 3.5 R_J), Nenon2017 reexamined the role of Io (and its neutral and plasma environments) and wave activity in the middle magnetosphere. Contrary to previous studies, the wave-electron interaction beyond Io's orbit was found by Nenon2017 to be a more efficient pitch-angle diffusion mechanism rather than an efficient gyro-resonant acceleration mechanism (e.g., Horne2008). In Nenon2017, the combined interactions of Io's neutral and plasma environments and waves with charged particles cause depletions in electron fluxes in the middle magnetosphere (~ 6-9.5 R_J) and the amount of electrons transported in the inner magnetosphere is subsequently lessened to a level comparable to past missions' in-situ measurements.

The magnetic field, particle, and radio measurements made by Juno during the first science orbits confirmed strong discrepancies between magnetic and particle and radio measurements and models, with differences of ~ 2-3 Gauss for the magnetic field, by up to an order of magnitude for the particle observations, and within a factor ~ 2-3 with Juno's measurements of Jupiter's electron-belt synchrotron emission (e.g., Bolton2017, Becker2017, SantosCosta2017). Due to the conflictual nature of modeling results on the wave-particle interaction and surprising first results of Juno at Jupiter close to the planet ($\sim< 2$ R_J), what are the sources and control parameters of the dynamical behavior of Jupiter's energetic electron populations in both the middle and inner magnetospheres still remain open questions.

In the present work, physics-based and empirical models have been merged to investigate the energy and spatial distributions of Jupiter's energetic and radiation-belt electron populations in the inner and middle magnetospheric regions (Fig. D1-4).

D3. MODEL RESULTS

D3-a Region beyond L ~5

Beyond 5 R_J, the distributions of keV to MeV electrons are defined by the variables *I* and *i*, the integral and differential directional intensities (after Divine&Garrett1983). These variables are function of local pitch-angle α, field strength B (equatorial B_e, at mirroring point B_m, and loss cone B_c) and E for given values of L:

$$\log I = A_0 - A_1 \log E + \frac{1}{2}(A_1 - A_2) \log\left[1 + (E/D_2)^2\right] + \frac{1}{3}(A_2 - A_3) \log\left[1 + (E/D_3)^3\right]$$

$$i = -\frac{dI}{dE} = \frac{I}{E}\left[A_1 + \frac{A_2 - A_1}{1 + (D_2/E)^2} + \frac{A_3 - A_2}{1 + (D_3/E)^3}\right]$$

where

$$A_n = a_n + (b_n - a_n)\,\frac{3\,(c_n - 1)^2\,x + 3\,(c_n - 1)\,c_n x^2 + c_n^2 x^3}{3 - 9c_n + 7c_n^2}$$

$$x = \frac{\log\,(B_m/B_e)}{\log\,(B_c/B_e)}$$

The local electron omnidirectional fluxes J and j are defined as follows:

$$J = 4\pi \int_0^{\pi/2} I(\sin\alpha)\,d\alpha$$

$$j = 4\pi \int_0^{\pi/2} i(\sin\alpha)\,d\alpha$$

To ease the empirical modeling of keV-MeV energy electrons for all latitudes at large radial distances (5-100 R_J), the M-shell parameter is used instead of L. This greatly speeds up the computation of electron distributions at any given spatial location (x0, y0, z0) in the magnetosphere, as M defines the distance from the planet to the point where the field line identified at (x0, y0, z0)

goes crossing the equatorial surface. M is determined using a field line tracing code (Fig. D1-3) and requires little computation time compared to the calculation of L-parameter. Note that typically M $\longrightarrow$ L as we approach the planet and M = L for a dipole.

We actually use Divine&Garrett1983's parametrization approach only for equatorial particles (x = 0 and $A_n = a_n$). The off-equatorial distributions depend on the equatorial profiles and are constrained using Legendre polynomials: the differential directional intensities are then expressed as $\log_{10}(i(\alpha)) = \sum C_n P_n(\sin \alpha)$ (after Chen2014). The coefficients $C_{n=0,11}$ are energy and M-shell dependent, constrained from best fits to datasets.

Figure D1-5 illustrates some preliminary results that are compared to the GIRE model (e.g., Garrett2012) for different electron energies. Pioneer 10&11 datasets and samples of Juno JADE-E ambient background count rates (e.g., McComas2014, Allegrini2020) were used to constrain our empirical model. We combined Connerney2018 + Khurana2005 models to develop this first version.

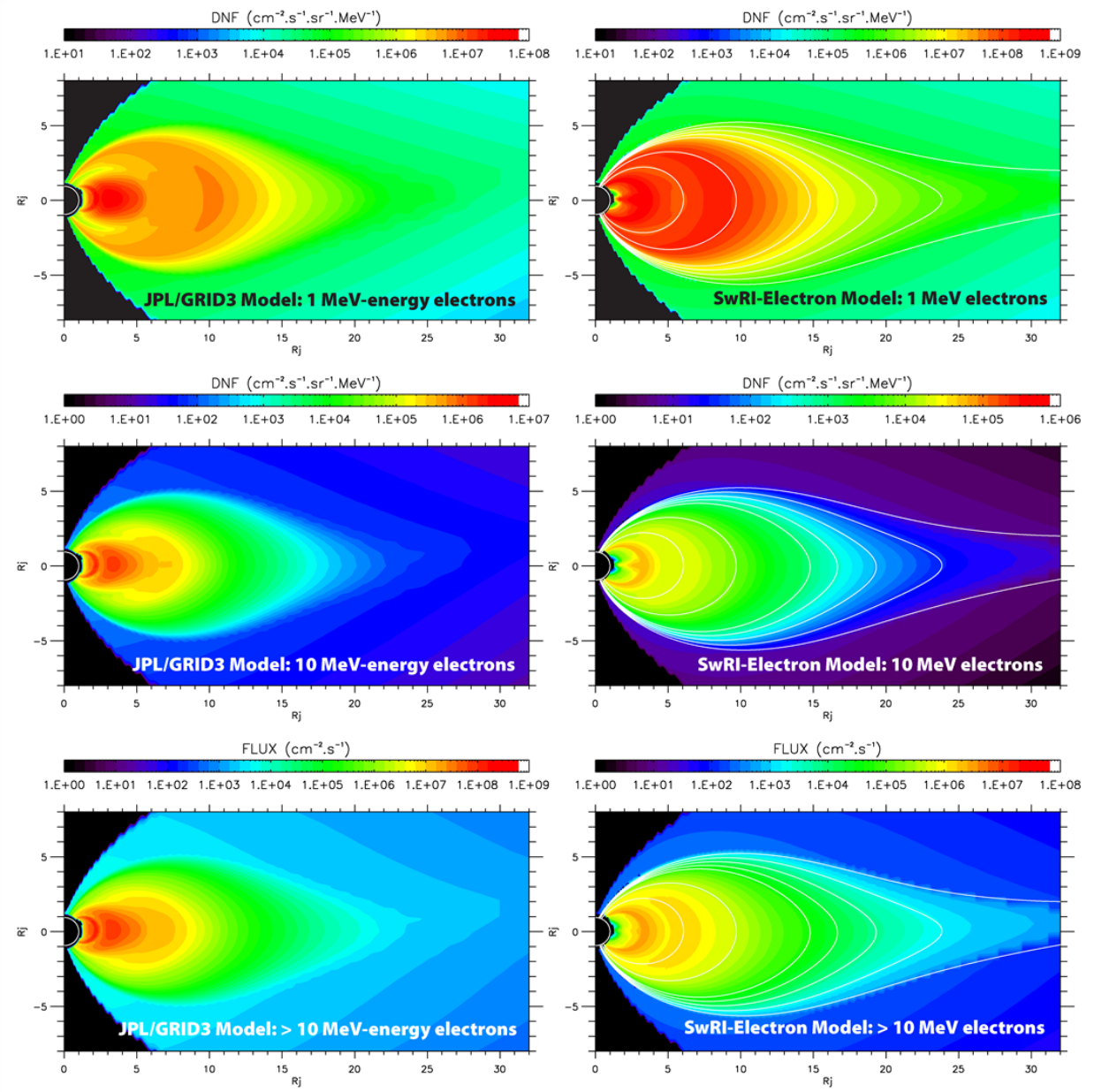

FIgure D1-5*: Intensity and Flux comparisons between JPL/GRID3 model (e.g., Garrett2012) and Southwest Research Institute's empirical model of energetic electron populations (SwRI/RM) for the region 1-100 R_J. Recent data processing indicated that SwRI/RM's first version were overestimating electron fluxes for energies ~< 1-3 MeV.*

We are currently merging Pioneer 10&11 GTT datasets, Juno JADE-E ambient background count rates from 2 dozens of Juno's orbits, and full Galileo EPD > 1.5 & 11.5 MeV datasets to refine our empirical modeling of keV-MeV energy electrons beyond 5 R_J, using our latest magnetic field computation tool (Cf. Fig. D1-2).

This empirical model is used to constrain our physical modeling of energetic electrons inside Io's orbit at the outer boundary (L = 5).

D3-b Region inside L ~ 5

To improve model comparisons with in-situ and ground-based observations in the innermost region of Jupiter's magnetosphere (L ~ < 5), we model the distribution of energetic and radiation-belt electrons using the diffusion theory concept described in Section B2. We use SwRI-RM empirical model primarily developed for the region ~5-100 R_J to constrain our physics-based model at L = 5. SantosCosta&Bolton2008's physics-based model is thus updated, starting with the implementation of SwRI's magnetic field computation tool (Cf. Fig. D1-2). The mechanisms accounted for the 1-5 L region are summarized in Fig. D1-6. Their modeling are summarized as follows:

- D_{LL} expression determined for the Kronian case as a function of L, E and α (Fig. C1-5) had been tested for the Jovian case. Simulation results do not show significant differences with a radial diffusion coefficient of the form $D_{LL} = D_o L^{3-4}$;

- The theoretical modeling of the interaction with moons and dust particles and synchrotron mechanism is similar to the works of SantosCosta&Bolton2008 and SantosCosta2003 and references therein.

- The main characteristics for moons and ring system taken into account in our modeling are summarized at these links: "Jovian Satellite Fact Sheet (https://nssdc.gsfc.nasa.gov/planetary/factsheet/joviansatfact.html)" & "Jovian Rings Fact Sheet (https://nssdc.gsfc.nasa.gov/planetary/factsheet/jupringfact.html)". A schematic view of Jupiter's inner moons and ring system is provided "here (https://en.wikipedia.org/wiki/Rings_of_Jupiter#/media/File:PIA01627_Ringe.jpg)".

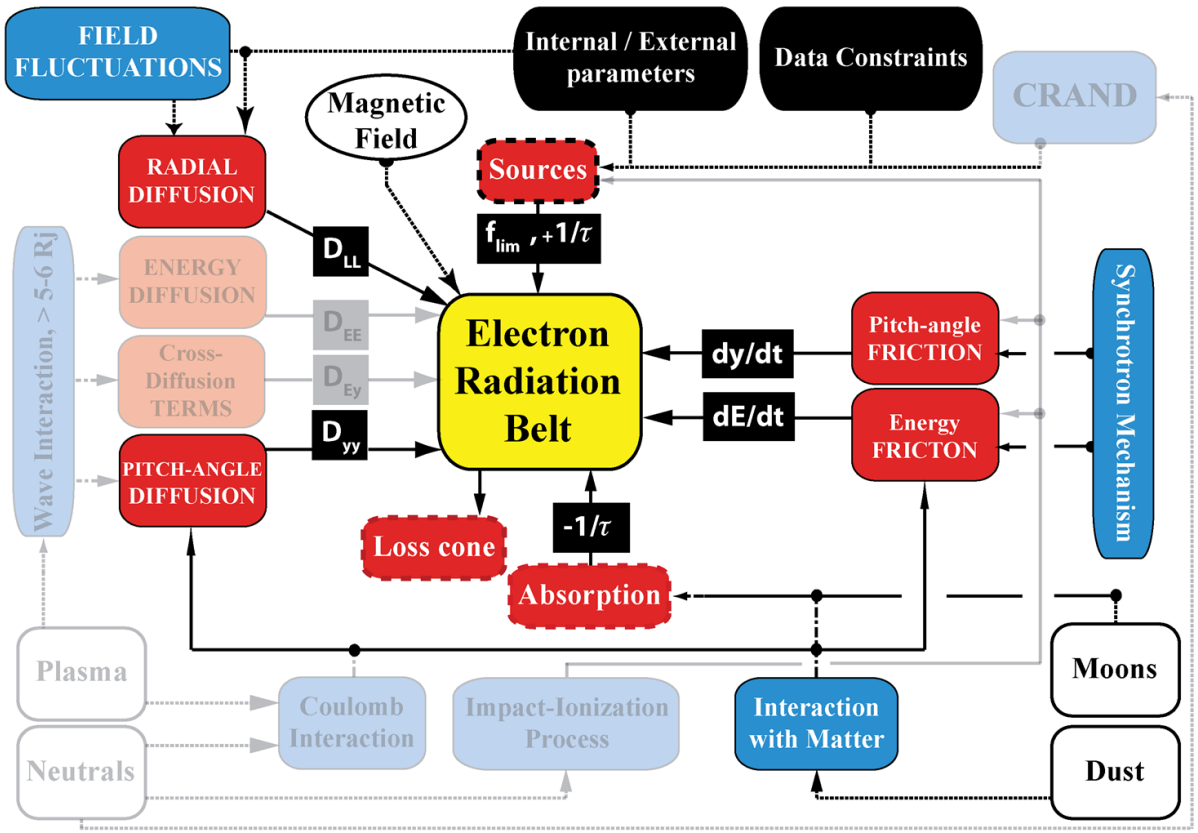

FIgure D1-6*: Theoretical approach for the three-dimensional modeling of Jupiter's electron radiation belt. Fields with 30% transparency indicate the processes that are either considered as secondary, contribute to total losses (i.e., Coulomb interaction with neutrals in the upper atmosphere) or not yet modeled.*

Figure D1-7 presents comparison results with datasets for the region L < 15, which is modeled with a physics-based model for L ~< 5 and empirical approach for L >~ 5 (Cf. D3-a). Model results show noticeable discrepancies within the halo and Amalthea's & Thebe's gossamer rings for the highest energies, regions where (1) interaction with dust particles may be underestimated due to unknown dust particle sizes and densities or (2) the interaction of waves (e.g., Z mode wave (e.g., Roussos2019)) generated or not by dusty plasmas (e.g., dust whistler-mode waves (Jafari2016)) may be missing.

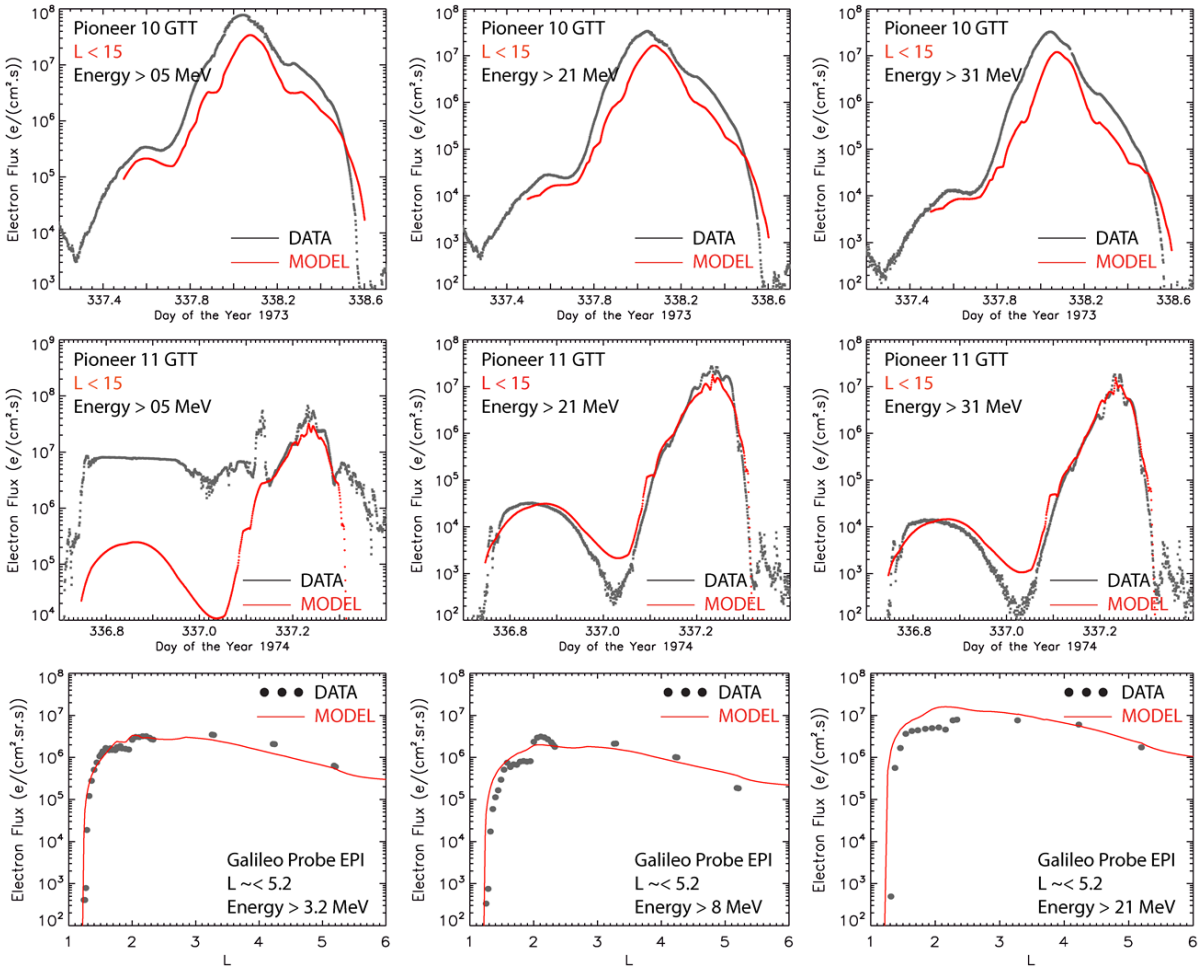

FIgure D1-7*: (top panels) Comparisons between Pioneer 10 GTT measurements and model of radiation-belt electron distributions for energies > 5, 21 and 31 MeV and L < 15. (middle panels) Comparisons between Pioneer 11 GTT measurements and model of radiation-belt electron distributions for energies > 5, 21 and 31 MeV and L < 15. (Bottom) Comparisons between Galileo Probe EPI measurements and model of radiation-belt electron distributions for energies > 3.2, 8 and 21 MeV and L ~< 5.2.*

E. MODELING URANUS' ENERGETIC ELECTRON ENVIRONMENT

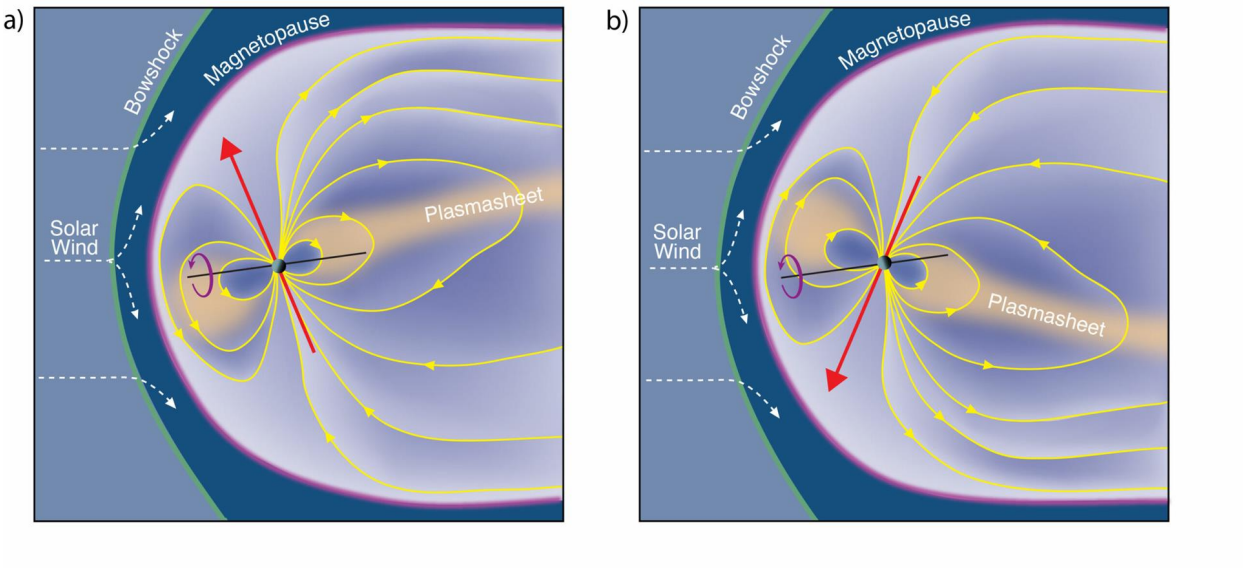

FIgure E1-1*: Schematic view of Uranus' Magnetosphere during Voyager 2 flyby in January 1986. Credit: Fran Bagenal & Steve Bartlett (https link to image (https://lasp.colorado.edu/home/mop/files/2020/11/Uranus_1986-scaled.jpg)).*

E1. MAGNETIC FIELD MODEL

The Voyager 2 measurements at Uranus have revealed a remarkable planetary magnetic field and magnetospheric configuration (e.g., Ness1991, Arridge2015). Nonetheless, Voyager 2 observations have shown that the Uranian magnetosphere as observed in January 1986 was in many respects similar to Earth's. Uranus' rotation axis lies essentially in the ecliptic plane and points roughly toward the Sun during the Voyager 2 era (e.g., Ness1991, Voigt1987, Behannon1987). The magnetic dipole axis is inclined by a large angle of ~60º with respect to the rotation axis (see Figure E1-1), so that the actual dipole tilt angle Ψ, measured from the z axis in a rotating Planet-centered Solar Magnetospheric coordinate system, varies in the range $22^o < \Psi < 38^o$. These values are similar to Earth's dipole tilt $\Psi_{Earth} < |35^o|$. The similar tilt angles, together with the lack of a sizable internal plasma source, such as Io in Jupiter's magnetosphere, lead to Voyager 2's observations of an "Earth-type" bipolar geomagnetic tail at Uranus, with lobes separated by a cross-tail current and plasma sheet (e.g., Ness1986; Behannon1987). The magnetospheric configuration observed during Voyager 2's flyby is expected to change drastically over the course of a Uranian year (e.g., Voigt1983, Schulz&McNab1996, Voigt1986, Voigt1987, Arridge2015).

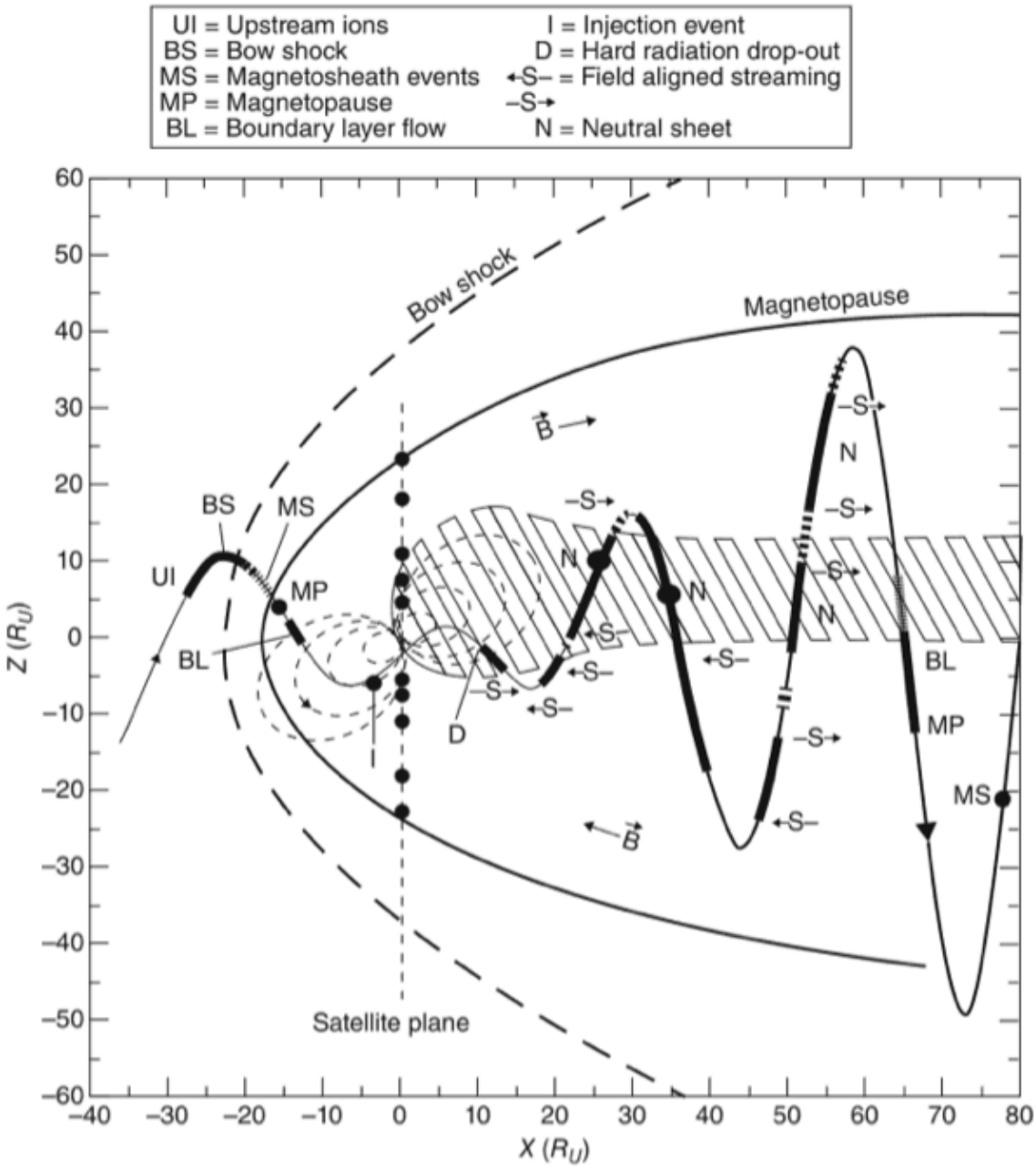

FIgure E1-2*: Trajectory of Voyager 2 through the Uranian magnetospehere in a rotating solar magnetospheric coordinate system summarizing the energetic particle results from Voyager 2 (from Mauk1987; Credit Arridge2015, Figure 7.10).*

In contrast to Earth's, however, Uranus' entire magnetosphere rotates by 360º within 17.24 hours (Desch1986). The magnetic moment of the dipole term was found to be 0.23 Gauss-R_U^3 (Ness1986, Connerney1987). The dipole axis 's tilt of 58.6º greatly exceeds that of Earth (~11º), Jupiter (~9.6º) and Saturn (~0º). The magnetic center was found to be displaced by 0.3 R_U from the planetary center, this being a significantly larger fraction of the planetary radius than the offsets for Earth, Jupiter and Saturn. The stagnation-point distance to the solar-wind magnetopause boundary was found to be ~18 R_U (see Figure E1-1; e.g., Voigt1987, Behannon1987, Lepping1987, Masters2014). The large angular separation between the dipole and rotation axes, in combination with the equatorial orbits of Uranus' major satellites (Miranda, Ariel, Umbriel, Tittania, Oberon), results in the complex and dynamic radiation-belt structure observed by Voyager 2 (e.g., Mauk1987, Cheng1991, Selesnick&Stone1991). The large inclination

of the Uranian rotation axis led to a spacial magnetic-tail configuration during Voyager era (e.g., Voigt1986, Voigt1987, Arridge2015).

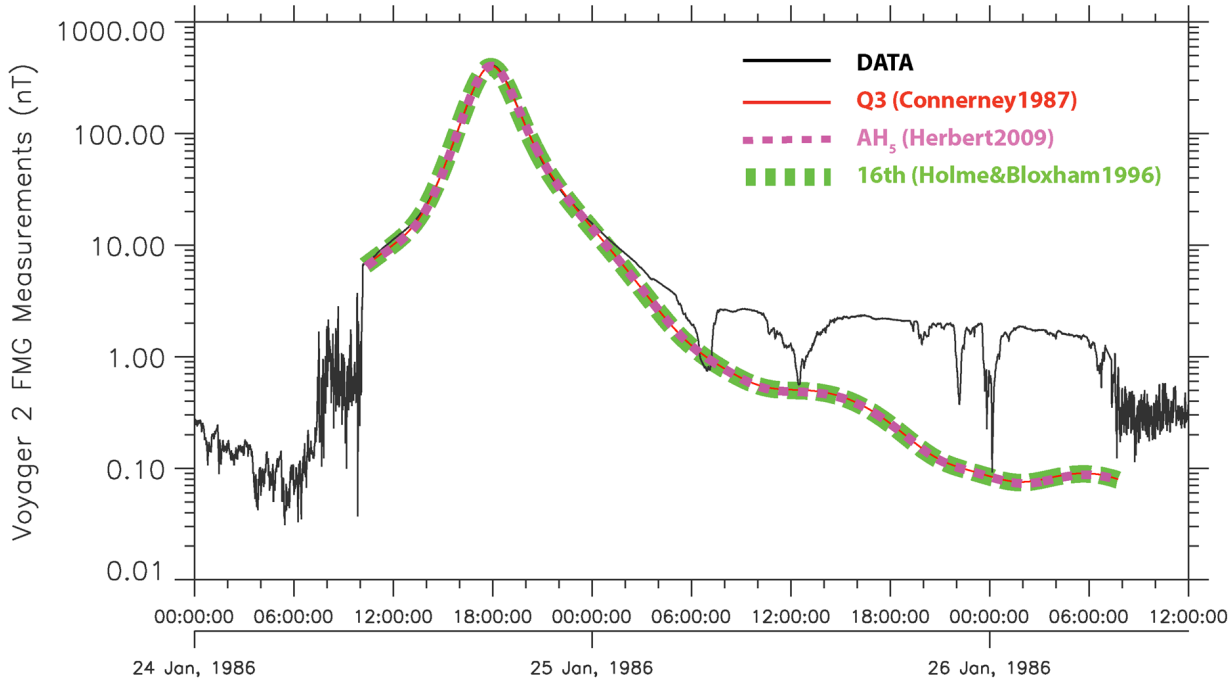

FIgure E1-3*: Magnitude of magnetic field (48-s averages) throughout Voyager 2's encounter while within the magnetosphere (~01-24-1986UT11:00 to ~01-25-1986UT07:00).*

Voyager 2 was located within a well-defined magnetosphere and magnetotail of the planet for 45 hr (e.g., Ness1986; Fig. E1-2). Nonetheless, about 12 hours (from 01-24-1986UT11:00 to 01-24-1986UT23:00) out of this period are pertinent for the investigation of charged trapped particle distributions at Uranus (e.g., Mauk1987, Cheng1991, Selesnick&Stone1991). A series of field models was developed based on Voyager-2's field measurements (e.g., Ness1986, Connerney1987, Holme&Bloxham1996, Herbert2009). For our region of interest, the Q_3 field model (Connerney1987) or any other models including higher multipole moments return comparable results (see Figure E1-3). The Q_3 model is used in our model as it was used to develop models of particle distributions at Uranus for the region $L < 15$ (e.g., Selesnick&Stone1991, Garrett2015).

E2. MOTIVATION FOR PHYSICS-BASED DEVELOPMENT

Launched in the 1970s to explore the gas giants Jupiter and Saturn, Voyager 2 remains the only robotic explorer in history to fly past Uranus (24 January 1986) and Neptune (25 August 1989), offering only a brief look at their planetary and magnetospheric systems (Fletcher2020a). The magnetospheres of the ice giants were found to be unique in our solar system, where highly unusual and time-variable interactions with the external solar wind are occurring. With the exception of remote observations of auroras, our understanding of the ice giants magnetospheres comes entirely from the in situ measurements from the Voyager spacecraft, combined with subsequent magnetospheric modeling.

Among others, Arridge2012, Arridge2014, Fletcher2020b, Kollmann2020 and Paty2020 have highlighted the merits to further explore the magnetospheric systems of the ice giants as part of future planetary missions that would combine orbital exploration of the planets, rings, satellites, alongside in situ atmospheric entry probe(s) and potentially landed elements on icy moons (Fletcher2020a). From a magnetospheric physics point of view, the Uranian system is the most fascinating of the ice giants. With the planet's high obliquity, Uranus system allows us to test our understanding of planetary magnetospheric dynamics and evolution to the extremes (Arridge&Paty2020).

Uranus' atypical magnetic configuration introduces intriguing questions (HessEtAl). Among those that are pertinent to the present study:

- To what extent is the Uranian magnetosphere driven by the solar wind versus internal processes? (Paty2020)
- How can Uranus have such intense radiation belts when it lacks a strong source population (Fig. E1-4)? (Kollmann2020)
- What role does the magnetosphere have in unusual ring structure and dynamics? (Kollmann2020)
- Can substorm-like injection phenomena be a source mechanism for Uranus' surprising intense MeV-energy electron radiation belts? (after Paty2020)
- How Uranus' energetic and radiation-belt electron populations dynamically evolve over the course of a Uranian year? (after Paty2020)

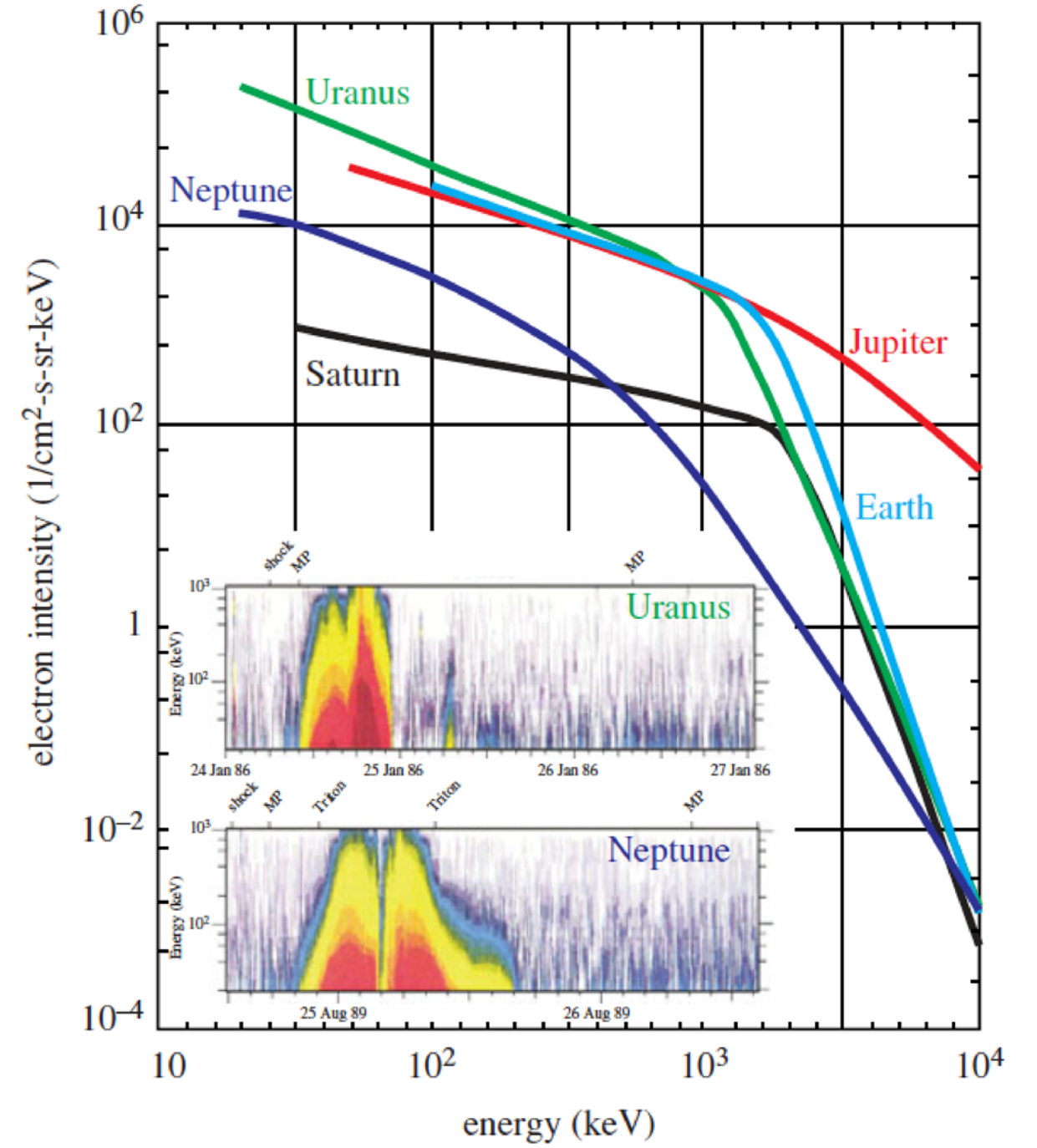

FIgure E1-4*: The most intense observed spectra of electron radiation belts of the ice giants compared to those found in other Solar System magnetospheres. The inset shows the spectrograms of energetic electrons observed at Uranus and Neptune by Voyager 2 (from Mauk&Fox2010) (Credit Paty2020, Fig. 3).*

In order to address some of these questions, we develop a physics-based model similar to Sections C & D. We here present the early stage of our effort to develop a self-consistent physical model of energetic and radiation-belt electron populations at Uranus (see Section E3). Until the present work, only a detailed analysis of Voyager 2's observations of energetic and radiation-belt populations were carried out by Mauk1987 and Selesnick&Stone1991.

Selesnick&Stone1991 also presented model fits to the differential intensity spectra from observations between L values of 6 and 15. Using the results from Mauk1987 and Selesnick&Stone1991, Garrett2015 developed empirical models of the high energy electron and proton environments for engineering design. Figure E1-5 presents a sample of Garrett2015's model outputs. Note that Garrett2015's model does not provide any information on the radial and latitudinal distributions of high energy charged particle environments inside ~4.2 R_U, due to an absence of data close to the planet.

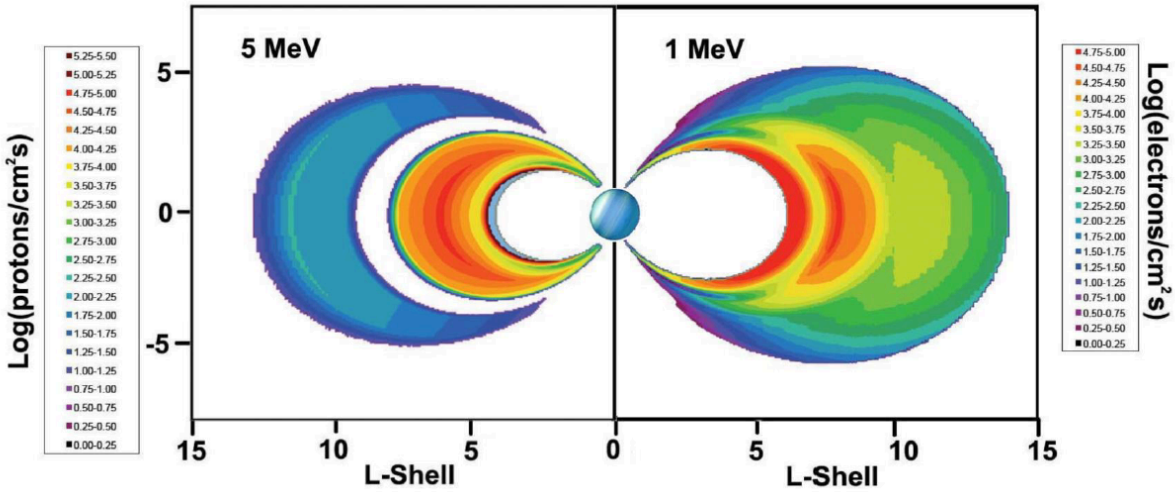

FIgure E1-5*: A plot of the 1-MeV electron and 5-MeV proton fluxes for a meridian profile (e.g., idealized dipole coordinates radial distance-latitude) of the Uranian radiation belts. Note that there is an absence of data inside ~4.2 R_U that prevents to model the high energy charged particle environments close to the planet (from Garrett2015).*

Our objective is to complete our current knowledge of how keV-MeV electrons are distributed between L values of 1 and 15, while investigating the key processes that shape the observed energy and spatial distributions.

E3. PHYSICS-BASED MODEL RESULTS

To understand and predict the distribution of keV-MeV electron populations between L values of 1 and 15, we compute the energy and spatial distributions using the diffusion theory concept described in Section B2. The mechanisms currently accounted for are:

- A source of warm, supra-thermal, energetic and radiation-belt electrons at our boundary condition L = 15 (See Fig. E1-6);

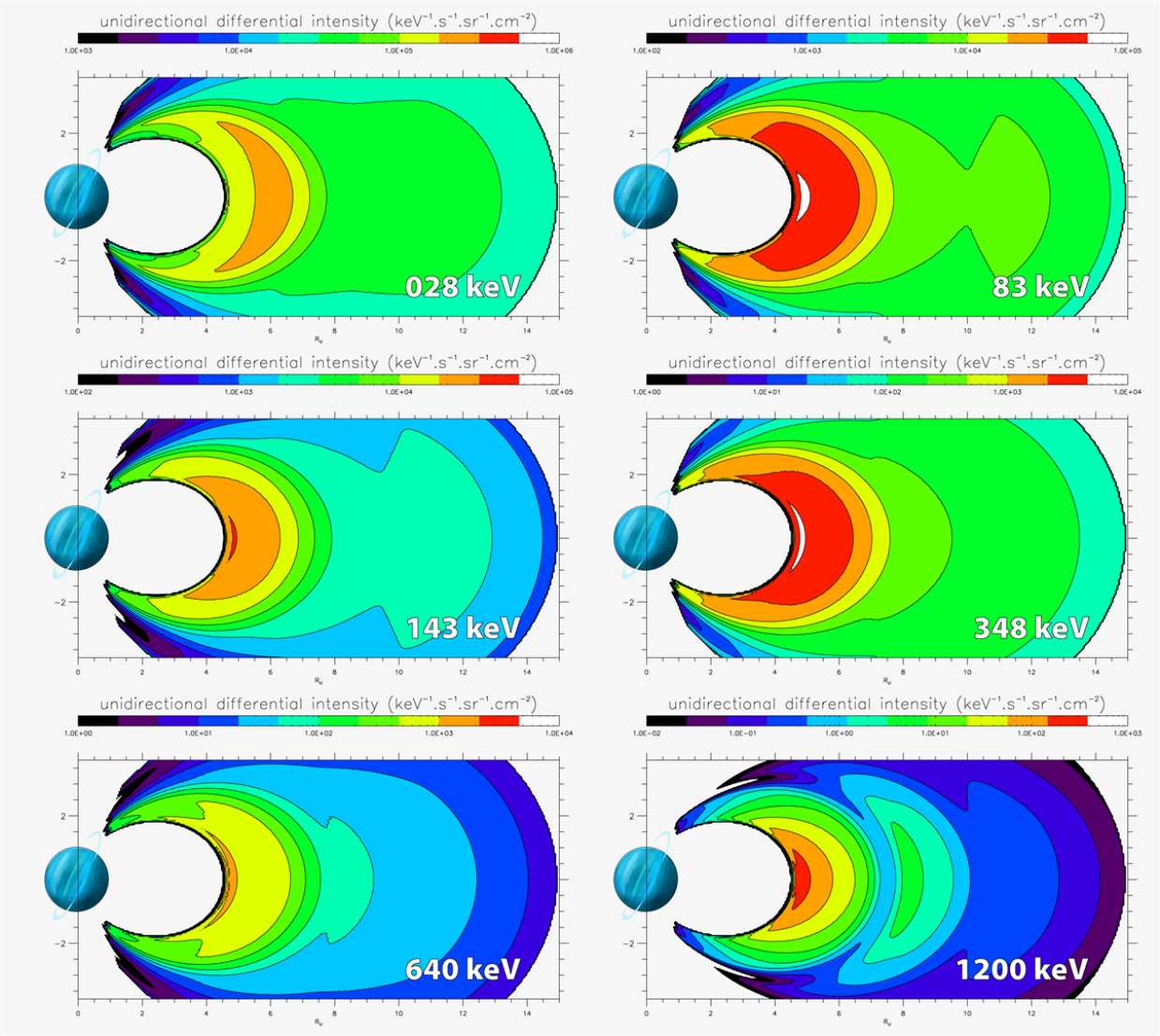

FIgure E1-6*: Cartography of energetic and radiation-belt electron intensities reconstructed from Voyager 2's in-situ measurements for the ~4.5-15 L region (after Mauk1987, Selesnick&Stone1991, Garrett2015).*

- D_{LL} expression for the Uranian case is of the form $D_{LL} = D_U L^n$. Power index n is energy dependent: n ~ 3-4 for supra-thermal electrons and n → 10 for 10s of MeV-energy electrons (after Cheng1987a, Hood1989, Cooper1990, Cooper&Stone1991 and Slesnick&Stone1991). Figure E1-7 presents model results when simulations account only for boundary conditions at L = 15 and adiabatic radial transport;

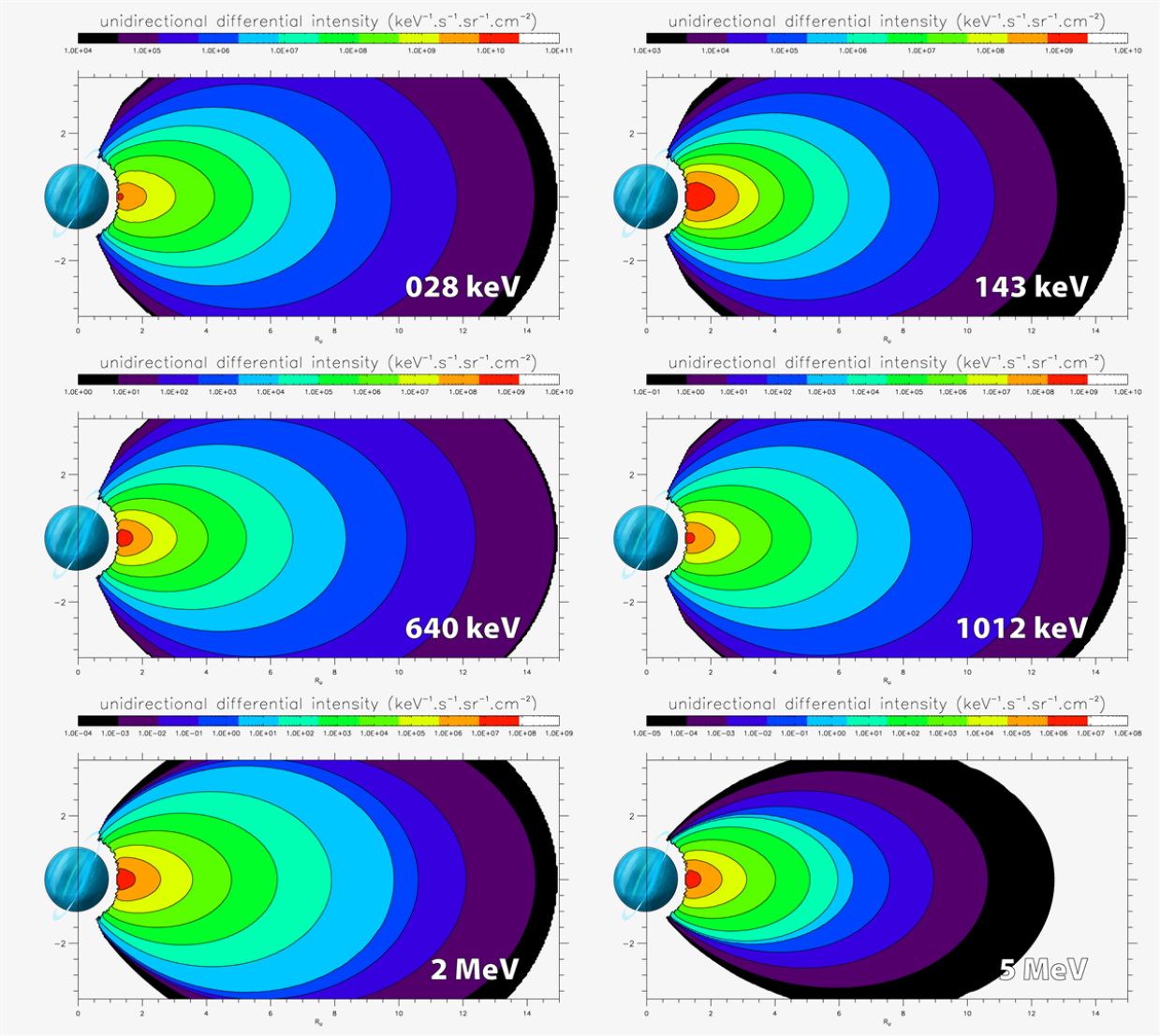

FIgure E1-7*: Computed distributions of energetic and radiation-belt electrons when model accounts only for boundary conditions at L = 15 and adiabatic radial transport.*

- Theoretical modeling of the interaction of electrons with 18 Uranian moons is similar to the works of SantosCosta&Bolton2008 and SantosCosta2003 and references therein. Satellites main characteristics are summarized @ "*Link to Uranian Satellite Fact Sheet (https://nssdc.gsfc.nasa.gov/planetary/factsheet/uraniansatfact.html)"*. Figure E1-8 presents model results when simulations account for boundary conditions at L = 15, adiabatic radial transport and moon sweeping effect.

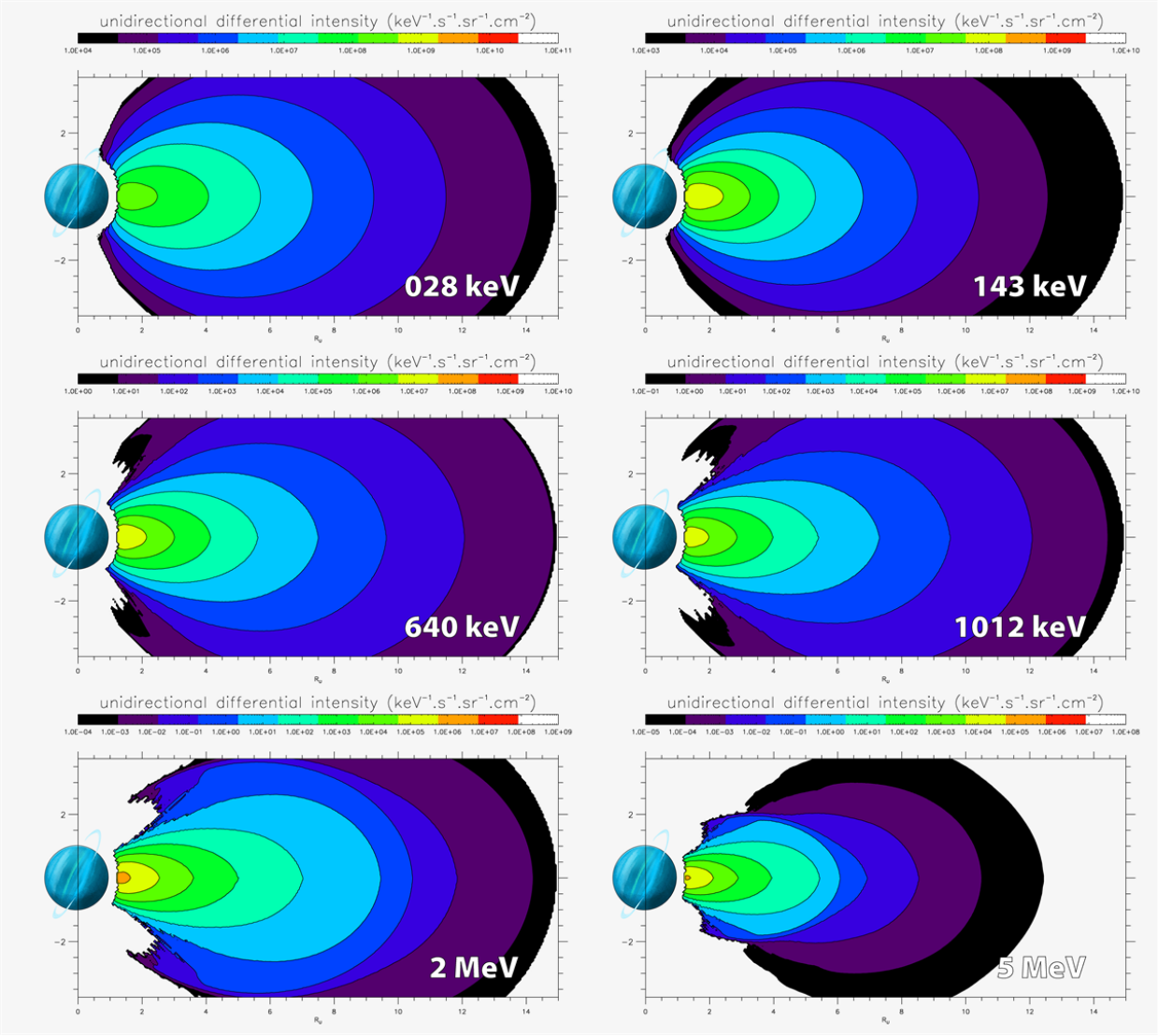

FIgure E1-8*: Computed distributions of energetic and radiation-belt electrons when model accounts for boundary conditions at L = 15, adiabatic radial transport and moon sweeping effect.*

F. SUMMARY

Data analyses of planetary missions had been carried out and used to develop (or improve) models of energetic and radiation-belt electron populations at Saturn, Jupiter and Uranus. Our key results are:

@ SATURN:

- Adiabatic transport cannot entirely explain the radial and angular features of warm to energetic electrons within Saturn's ~2-15 R_S region. Simulation results suggest a transport mechanism dependent of radial distance, energy and pitch-angle. The radial transport may be governed by the particle energy;

- Beyond ~2.3 R_S, interactions with cold plasma and dust particles play a secondary role on the distribution of electrons with energies greater than 10's of keV;

- The combined effect of adiabatic radial transport, collision with neutrals and interaction with waves significantly reshape the radial, energy and angular distributions of energetic electrons at Saturn;

- A source of supra-thermal electrons at high-latitudes is required in our simulations to maintain the field-aligned features observed beyond ~10 R_S; Interchange injection events permit to replenish the supra-thermal electron populations in the region ~4-10 R_S.

@ JUPITER:

- The Divine&Garrett1983 empirical model of energetic to relativistic electron populations had been revisited for the region ~5-100 R_J, using the latest published model of planetary field, and median and outer magnetospheric field models. Further work is required to refine the new empirical model in order to develop a self-consistent model useful for data analyses, observation planning and mission concepts. This will be achieved by reconciling Galileo EPD particle measurements with Juno particle and radiation background datasets.

- SantosCosta&Bolton2008' s physical model of energetic and radiation-belt electron populations had been revisited. Comparisons with Pioneer GTT and Galileo EPI datasets suggest missing loss mechanism(s) inside ~2-3 R_J. Comparisons with remote observations of Jupiter's synchrotron emission and Juno's energetic and penetrating radiation datasets would provide further modeling constraints. Comparisons with data would also assist in determining the processes to be added in order to improve our latest model of Jupiter's energetic and radiation-belt electron populations. Revisiting the interaction with dust particles and implementing interaction with waves generated by dusty plasma could possibly be the next modeling step.

@ URANUS:

- Similarly to the Kronian case, adiabatic transport cannot explain the radial and angular features of warm to ultra-relativistic

electron populations within the ~1-15 L region. Simulation results support the idea that radial transport is radial distance and particle energy dependent (e.g., Cheng1987a, Hood1989 and Slesnick&Stone1991);

- Simulation results suggest that, with absence of loss mechanisms inside L = 15, energetic and radiation-belt electron populations would be higher by 1-3 orders of magnitude in intensity close to the planet (L ~ 1-8). Simulation results confirm that electron populations are swept during encounter with moons but there are other loss mechanisms dependent of radial, energy and pitch-angle to account for (e.g., Cooper1990, Cooper&Stone1991);

- To improve our modeling of Uranus' electron populations between L values of 1 and 15, interactions with Uranus' rings system (e.g., Gurnett1987; links to Uranian Rings Fact Sheet "1 (https://nssdc.gsfc.nasa.gov/planetary/factsheet/uranringfact.html)" & "2 (https://pds-rings.seti.org/uranus/uranus_tables.html)") and atomic hydrogen corona (e.g, Cheng1987b, Herbert1988, Herbert &Hall1996), and waves (e.g., Coroniti1987, Kurth1987, Kurth1991) inward of L ~ 8-10 will be investigated.

DISCLOSURES

Key data analysis, theoretical modeling, and numerical computational tasks for Saturn were carried out at Southwest Research Institute under NASA GSFC grant 80NSSC18K1100. The development at Southwest Research Institute of a data processing and analysis tool of Cassini CAPS ELS observations had benefited from the support of the Cassini CAPS team during the Cassini prime and extended missions (NASA JPL subcontracts 1243218 and 1356497).

Data analysis, theoretical modeling, and numerical computational tasks were carried out at Southwest Research Institute for Jupiter. The work is sponsored by NASA MSFC in support of the Juno mission under contract NNM06AA75C.

Data analysis, theoretical modeling, and numerical computational tasks for Uranus were carried out by adapting the Kronian and Jovian modeling tools developed at Southwest Research Institute to the Uranian environment.

All data sets used in this work are publicly available at the NASA Planetary Data System website (http://pds.nasa.gov) or other public domain databases.

Authors thank Dr. K. Khurana for making available his outer planet magnetospheric field models for this work.

ABSTRACT

The in-situ magnetospheric exploration of the four large planets of our solar system had started with Pioneer 10's flyby of Jupiter in Dec. 1973. The second collection of field, particle and radio data of the gas giant was carried out by Pioneer 11 in Dec. 1974, before this spacecraft made its closest approach to Saturn in Sep. 1979. Around the same period, Voyager 1 (2) flew by Jupiter in Mar. (Jul.) 1979 then Saturn in Nov. (Aug.) 1980 (1981). As of today, only Voyager 2 visited the magnetospheres of Uranus (Jan. 1986) and Neptune (Aug. 1989). Galileo had remained the only spacecraft to orbit an outer planet for several years (1995 - 2003) until the arrival of Juno at Jupiter in 2016. Between 2004 and 2017, the Cassini mission had provided a wealth of in-situ data pertinent to the study of magnetospheric particles at Saturn. In this paper, we present our current understanding of the processes that shape the spatial distributions of energetic electrons trapped in the magnetospheres of Jupiter ($L < 6$), Saturn ($L < 15$) and Uranus ($L < 15$) obtained by combining multi-instrument analyses of data from past missions (Pioneer, Voyager, Galileo, Cassini) and computational models of charged particle fluxes. To determine what controls the energy and spatial distributions throughout the different magnetospheres, we compute the time evolution of particle distributions with the help of a diffusion theory particle transport code that solves the governing 3-D Fokker-Planck equation. Particle, field and wave datasets are either used to provide model constraints, assist in modeling physical processes, or validate our simulation results. We will emphasize our latest results regarding the relative (or coupled) role of mechanisms at Saturn, including the radial transport and interactions of electrons with Saturn's dust/neutral/plasma environments and waves, as well as particle sources from high-latitudes, interchange injections, and outer magnetospheric region. The lessons learned from our modeling of electron distributions at Saturn will be used to identify the processes that may be missing in our modeling of Jupiter's energetic electron environment or those in need to be implemented using new modeling concepts. Our first physics-based modeling of electron populations at Uranus will also be assessed with our data-model comparison approach.

REFERENCES

Achilleos2010: Achilleos, Nick, P. Guio, and Chris S. Arridge. A model of force balance in Saturn's magnetodisc. Monthly Notices of the Royal Astronomical Society 401.4 (2010): 2349-2371.

Acuna1976: Acuna, M. H., & Ness, N. F. (1976). The main magnetic field of Jupiter. Journal of Geophysical Research, 81 (16), 2917-2922.

Acuna1983: Acuna, M. H., Behannon, K. W., & Connemey, J. E. P (1983). Jupiter's magnetic field and magnetosphere. Physics of the Jovian Magnetosphere, edited by A.J. Dessler, 1-50.

Allegrini2020; Allegrini, F., Gladstone, G. R., Hue, V., Clark, G., Szalay, J. R., Kurth, W. S., ... & Greathouse, T. K. (2020). First report of electron measurements during a Europa footprint tail crossing by Juno. Geophysical Research Letters, 47 (18), e2020GL089732.

Arridge2008: Arridge, C. S., Khurana, K. K., Russell, C. T., Southwood, D. J., Achilleos, N., Dougherty, M. K., ... & Leinweber, H. K. (2008). Warping of Saturn's magnetospheric and magnetotail current sheets. Journal of Geophysical Research: Space Physics, 113 (A8).

Arridge2012: Arridge, C. S., Agnor, C. B., André, N., Baines, K. H., Fletcher, L. N., Gautier, D., ... & Mousis, O. (2012). Uranus Pathfinder: exploring the origins and evolution of Ice Giant planets. Experimental Astronomy, 33(2-3), 753-791.

Arridge2014: Arridge, C. S., Achilleos, N., Agarwal, J., Agnor, C. B., Ambrosi, R., André, N., ... & Bisi, M. M. (2014). The science case for an orbital mission to Uranus: exploring the origins and evolution of ice giant planets. Planetary and Space Science, 104, 122-140.

Arridge2015: Arridge, C. S. (2015). Magnetotails of Uranus and Neptune. Magnetotails in the Solar System, 207, 119-133.

Behannon1987: Behannon, K. W., Lepping, R. P., Sittler Jr, E. C., Ness, N. F., Mauk, B. H., Krimigis, S. M., & McNutt Jr, R. L. (1987). The magnetotail of Uranus. Journal of Geophysical Research: Space Physics, 92(A13), 15354-15366.

Bolton2017: Bolton, S. J., Adriani, A., Adumitroaie, V., Allison, M., Anderson, J., Atreya, S., ... & Folkner, W. (2017). Jupiter's interior and deep atmosphere: The initial pole-to-pole passes with the Juno spacecraft. Science, 356 (6340), 821-825.

Becker2017: Becker, H. N., Santos−Costa, D., Jørgensen, J. L., Denver, T., Adriani, A., Mura, A., ... & Alexander, J. W. (2017). Observations of MeV electrons in Jupiter's innermost radiation belts and polar regions by the Juno radiation monitoring investigation: Perijoves 1 and 3. Geophysical Research Letters, 44 (10), 4481-4488.

Bunce2007: Bunce, E. J., Cowley, S. W. H., Alexeev, I. I., Arridge, C. S., Dougherty, M. K., Nichols, J. D., & Russell, C. T. (2007). Cassini observations of the variation of Saturn's ring current parameters with system size. Journal of Geophysical Research: Space Physics, 112 (A10).

Carbary2011: Carbary, J. F., Mitchell, D. G., Paranicas, C., Roelof, E. C., Krimigis, S. M., Krupp, N., ... & Dougherty, M. (2011). Pitch angle distributions of energetic electrons at Saturn. Journal of Geophysical Research: Space Physics, 116 (A1).

Chen2014: Chen, Y., Friedel, R. H., Henderson, M. G., Claudepierre, S. G., Morley, S. K., & Spence, H. E. (2014). REPAD: An empirical model of pitch angle distributions for energetic electrons in the Earth's outer radiation belt. Journal of Geophysical Research: Space Physics, 119(3), 1693-1708.

Cheng1987a: Cheng, A. F., Krimigis, S. M., Mauk, B. H., Keath, E. P., Maclennan, C. G., Lanzerotti, L. J., ... & Armstrong, T. P. (1987). Energetic ion and electron phase space densities in the magnetosphere of Uranus. Journal of Geophysical Research: Space Physics, 92(A13), 15315-15328.

Cheng1987b: Cheng, A. F. (1987). Proton and oxygen plasmas at Uranus. Journal of Geophysical Research: Space Physics, 92 (A13), 15309-15314.

Cheng1991: Cheng, A. F., Krimigis, S. M., & Lanzerotti, L. J. (1991). Energetic Particles at Uranus, Uranus JT Bergstralh, ED Miner, MS Matthews, 831–893, Univ. of Ariz. Press, Tucson.

Clark2014: Clark, G., Paranicas, C., Santos-Costa, D., Livi, S., Krupp, N., Mitchell, D. G., ... & Tseng, W. L. (2014). Evolution of electron pitch angle distributions across Saturn's middle magnetospheric region from MIMI/LEMMS. Planetary and Space Science, 104, 18-28.

Clark2018: Clark, G., Tao, C., Mauk, B. H., Nichols, J., Saur, J., Bunce, E. J., ... & Bonfond, B. (2018). Precipitating electron energy flux and characteristic energies in Jupiter's main auroral region as measured by Juno/JEDI. Journal of Geophysical Research: Space Physics, 123 (9), 7554-7567.

Connerney1981a: Connerney, J. E. P. (1981). The magnetic field of Jupiter: A generalized inverse approach. Journal of Geophysical Research: Space Physics, 86 (A9), 7679-7693.

Connerney1981b: Connerney, J. E. P., Acuna, M. H., & Ness, N. F. (1981). Modeling the Jovian current sheet and inner magnetosphere. Journal of Geophysical Research: Space Physics, 86 (A10), 8370-8384.

Connerney1982: Connerney, J. E. P., N. F. Ness, and M. H. Acuna. Zonal harmonic model of Saturn's magnetic field from Voyager 1 and 2 observations. Nature 298.5869 (1982): 44-46.

Connerney1983: Connerney, J. E. P., M. H. Acuna, and N. F. Ness. Currents in Saturn's magnetosphere. Journal of Geophysical Research: Space Physics 88.A11 (1983): 8779-8789.

Connerney1984: Connerney, J. E. P., L. Davis Jr, and D. L. Chenette. Magnetic field models. Saturn book (1984): 354-377.

Connerney1987: Connerney, J. E. P., Acuña, M. H., & Ness, N. F. (1987). The magnetic field of Uranus. Journal of Geophysical Research: Space Physics, 92 (A13), 15329-15336.

Connerney1993: Connerney, J. E. P. (1993). Magnetic fields of the outer planets. Journal of Geophysical Research: Planets, 98 (E10), 18659-18679.

Connerney2018: Connerney, J. E. P., Kotsiaros, S., Oliversen, R. J., Espley, J. R., Jørgensen, J. L., Joergensen, P. S., ... & Bolton, S. J. (2018). A new model of Jupiter's magnetic field from Juno's first nine orbits. Geophysical Research Letters, 45 (6), 2590-2596.

Connerney2020: Connerney, J. E. P., Timmins, S., Herceg, M., & Joergensen, J. L. (2020). A Jovian Magnetodisc Model for the Juno Era. Journal of Geophysical Research: Space Physics, 125 (10), e2020JA028138.

Cooper1990: Cooper, J. F. (1990). Satellite sweeping of electrons at Neptune and Uranus. Geophysical research letters, 17 (10), 1665-1668.

Cooper&Stone1991: Cooper, J. F., & Stone, E. C. (1991). Electron signatures of satellite sweeping in the magnetosphere of Uranus. Journal of Geophysical Research: Space Physics, 96 (A5), 7803-7821.

Coroniti1987: Coroniti, F. V., Kurth, W. S., Scarf, F. L., Krimigis, S. M., Kennel, C. F., & Gurnett, D. A. (1987). Whistler mode emissions in the Uranian radiation belts. Journal of Geophysical Research: Space Physics, 92(A13), 15234-15248.

dePater1981a: de Pater, I. (1981). A comparison of the radio data and model calculations of Jupiter's synchrotron radiation, 1. The high energy electron distribution in Jupiter's inner magnetosphere. Journal of Geophysical Research: Space Physics, 86 (A5), 3397-3422.

dePater1981b: de Pater, I. (1981). A comparison of radio data and model calculations of Jupiter's synchrotron radiation 2. East−west asymmetry in the radiation belts as a function of Jovian longitude. Journal of Geophysical Research: Space Physics, 86 (A5), 3423-3429.

dePater1994: De Pater, I., & Goertz, C. K. (1994). Radial diffusion models of energetic electrons and Jupiter's synchrotron radiation: 2. Time variability. Journal of Geophysical Research: Space Physics, 99 (A2), 2271-2287.

dePater1997: de Pater, I., Schulz, M., & Brecht, S. H. (1997). Synchrotron evidence for Amalthea's influence on Jupiter's electron radiation belt. Journal of Geophysical Research: Space Physics, 102 (A10), 22043-22064.

Desch1986: Desch, M. D., Connerney, J. E. P., & Kaiser, M. L. (1986). The rotation period of Uranus. Nature, 322(6074), 42-43.

deSoriaSantacruz2016: de Soria−Santacruz, M., Garrett, H. B., Evans, R. W., Jun, I., Kim, W., Paranicas, C., & Drozdov, A. (2016). An empirical model of the high−energy electron environment at Jupiter. Journal of Geophysical Research: Space Physics, 121 (10), 9732-9743.

Divine&Garrett1983: Divine, N., and Garrett, H.~B. (1983). Charged particle distributions in Jupiter's magnetosphere. Journal of Geophysical Research, 88, 6889--6903.

Dougherty2004: Dougherty, M. K., et al. The Cassini magnetic field investigation. The cassini-huygens mission. Springer, Dordrecht, 2004. 331-383.

Ezoe2010: Ezoe, Y., Ishikawa, K., Ohashi, T., Miyoshi, Y., Terada, N., Uchiyama, Y., & Negoro, H. (2010). Discovery of diffuse hard X-ray emission around Jupiter with Suzaku. The Astrophysical Journal Letters, 709 (2), L178.

Fischer1996: Fischer, H. M., et al. High-energy charged particles in the innermost Jovian magnetosphere. Science 272.5263 (1996): 856-858.

Fletcher2020a: Fletcher LN, Simon AA, Hofstadter MD, Arridge CS, Cohen IJ, Masters, A, Mandt K, Coustenis A. (2020). Ice giant system exploration in the 2020s: an introduction. Phil. Trans. R. Soc. A 378: 20190473. http://dx.doi.org/10.1098/rsta.2019.0473.

Fletcher2020b: Fletcher, L. N., Helled, R., Roussos, E., Jones, G., Charnoz, S., André, N., ... & Ferri, F. (2020). Ice Giant Systems: The scientific potential of orbital missions to Uranus and Neptune. Planetary and Space Science, 105030.

Garrett2003: Garrett, H. B., Jun, I., Ratliff, J. M., Evans, R. W., Clough, G. A., & McEntire, R. W. (2003). Galileo measurements of the Jovian electron radiation environment.

Garrett2005: Garrett, H. B., Levin, S. M., Bolton, S. J., Evans, R. W., & Bhattacharya, B. (2005). A revised model of Jupiter's inner electron belts: Updating the Divine radiation model. Geophysical research letters, 32 (4).

Garrett2012: Garrett, H. B., Kokorowski, M., Jun, I., & Evans, R. W. (2012). Galileo interim radiation electron model: Update —2012. Pasadena, CA: Jet Propulsion Laboratory, National Aeronautics and Space Administration, 2012.

Garrett2015: Garrett, H., Martinez-Sierra, L. M., & Evans, R. (2015). The JPL uranian radiation model (UMOD). Pasadena, CA: Jet Propulsion Laboratory, National Aeronautics and Space Administration, 2015.

Gurnett1987: Gurnett, D. A., Kurth, W. S., Scarf, F. L., Burns, J. A., Cuzzi, J. N., & Grün, E. (1987). Micron−sized particle impacts detected near Uranus by the Voyager 2 plasma wave instrument. Journal of Geophysical Research: Space Physics, 92 (A13), 14959-14968.

Gurnett2004: Gurnett, D. A., et al. The Cassini radio and plasma wave investigation. The Cassini-Huygens Mission. Springer, Dordrecht, 2004. 395-463.

Herbert1988: Herbert, F. (1988). Constraints on the neutral hydrogen corona at Uranus from its interaction with magnetospheric plasma. Geophysical Research Letters, 15 (7), 705-708.

Herbert &Hall1996: Herbert, F., & Hall, D. T. (1996). Atomic hydrogen corona of Uranus. Journal of Geophysical Research: Space Physics, 101 (A5), 10877-10885.

Herbert2009: Herbert, F. (2009). Aurora and magnetic field of Uranus. Journal of Geophysical Research: Space Physics, 114 (A11).

HessEtAl: Hess, S. et al. Exploration of the Uranus magnetosphere. White paper : Solar and Heliosphere Physics Decadal Survey 2013-20 @ http://www8.nationalacademies.org/SSBSurvey/DetailFileDisplay.aspx?id=712&parm_type=HDS.

Holme1996: Holme, R., & Bloxham, J. (1996). The magnetic fields of Uranus and Neptune: Methods and models. Journal of Geophysical Research: Planets, 101(E1), 2177-2200.

Hood1989: Hood, L. L. (1989). Radial diffusion in the Uranian radiation belts: Inferences from satellite absorption loss models. Journal of Geophysical Research: Space Physics, 94 (A11), 15077-15088.

Horanyi2008: Horányi, M., Juhász, A., & Morfill, G. E. (2008). Large−scale structure of Saturn's E−ring. Geophysical research letters, 35 (4).

Horne2008: Horne, R. B., Thorne, R. M., Glauert, S. A., Menietti, J. D., Shprits, Y. Y., & Gurnett, D. A. (2008). Gyro-resonant electron acceleration at Jupiter. Nature Physics, 4 (4), 301-304.

Jafari2016: Jafari, S. (2016). Interaction of energetic electrons with dust whistler-mode waves in magnetospheric dusty plasmas. Astrophysics and Space Science, 361 (4), 134.

Jun2003: Jun, I., Garrett, H. B., Swimm, R., Evans, R. W., & Clough, G. (2005). Statistics of the variations of the high-energy electron population between 7 and 28 jovian radii as measured by the Galileo spacecraft. Icarus, 178 (2), 386-394.

Jun2019: Jun, I., Garrett, H. B., & Evans, R. W. (2019). Trapped particle environments of the outer planets. IEEE Transactions on Plasma Science, 47 (8), 3923-3930.

Krimigis2004: Krimigis, S. M., et al. Magnetosphere imaging instrument (MIMI) on the Cassini mission to Saturn/Titan. The Cassini-Huygens Mission. Springer, Dordrecht, 2004. 233-329.

Khurana1992: Khurana, K. K. (1992). A generalized hinged−magnetodisc model of Jupiter's nightside current sheet. Journal of Geophysical Research: Space Physics, 97 (A5), 6269-6276.

Khurana1997: Khurana, K. K. (1997). Euler potential models of Jupiter's magnetospheric field. Journal of Geophysical Research: Space Physics, 102 (A6), 11295-11306.

Khurana2005: Khurana, K. K., & Schwarzl, H. K. (2005). Global structure of Jupiter's magnetospheric current sheet. Journal of Geophysical Research: Space Physics, 110 (A7).

Khurana2007: Khurana, K. K., Arridge, C. S., Schwarzl, H., & Dougherty, M. K. (2006). A model of Saturn's magnetospheric field based on latest Cassini observations. AGUSM, 2007, P44A-01.

Khurana2009: Khurana, K. K., Mitchell, D. G., Arridge, C. S., Dougherty, M. K., Russell, C. T., Paranicas, C., ... & Coates, A. J. (2009). Sources of rotational signals in Saturn's magnetosphere. Journal of Geophysical Research: Space Physics, 114 (A2).

Kollmann2011: Kollmann, P., Roussos, E., Paranicas, C., Krupp, N., Jackman, C. M., Kirsch, E., & Glassmeier, K. H. (2011). Energetic particle phase space densities at Saturn: Cassini observations and interpretations. Journal of Geophysical Research: Space Physics, 116 (A5).

Kollmann2018: Kollmann, P., Roussos, E., Paranicas, C., Woodfield, E. E., Mauk, B. H., Clark, G., ... & Vandegriff, J. (2018). Electron acceleration to MeV energies at Jupiter and Saturn. Journal of Geophysical Research: Space Physics, 123 (11), 9110-9129.

Kollmann2020: Kollmann, P., Cohen, I., Allen, R. C., Clark, G., Roussos, E., Vines, S., ... & Cartwright, R. (2020). Magnetospheric studies: a requirement for addressing interdisciplinary mysteries in the ice giant systems. Space Science Reviews, 216(5), 1-26.

Kurth1987: Kurth, W. S., Barbosa, D. D., Gurnett, D. A., & Scarf, F. L. (1987). Electrostatic waves in the magnetosphere of Uranus. Journal of Geophysical Research: Space Physics, 92 (A13), 15225-15233.

Kurth1991: Kurth, W. S., Gurnett, D. A., Scarf, F. L., & Coroniti, F. V (1991). Wave-particle interactions in the magnetosphere of Uranus. In: Uranus, Ed. Bergstralh, Jay T. and Miner, Ellis D. and Matthews, Mildred S., 926-958.

Lepping1987: Lepping, R. P., Burlaga, L. F., & Klein, L. W. (1987). Surface waves on Uranus' magnetopause. Journal of Geophysical Research: Space Physics, 92 (A13), 15347-15353.

Levin2001: Levin, S. M., Bolton, S. J., Gulkis, S. L., Klein, M. J., Bhattacharya, B., & Thorne, R. M. (2001). Modeling Jupiter's synchrotron radiation. Geophysical research letters, 28 (5), 903-906.

Lorenzato2012: Lorenzato, L., Sicard, A., & Bourdarie, S. (2012). A physical model for electron radiation belts of Saturn. Journal of Geophysical Research: Space Physics, 117 (A8).

Masters2014: Masters, A. (2014). Magnetic reconnection at Uranus' magnetopause. Journal of Geophysical Research: Space Physics, 119 (7), 5520-5538.

Mauk1987: Mauk, B. H., Krimigis, S. M., Keath, E. P., Cheng, A. F., Armstrong, T. P., Lanzerotti, L. J., ... & Hamilton, D. C. (1987). The hot plasma and radiation environment of the Uranian magnetosphere. Journal of Geophysical Research: Space Physics, 92 (A13), 15283-15308.

Mauk&Fox2010: Mauk, B. H., & Fox, N. J. (2010). Electron radiation belts of the solar system. Journal of Geophysical Research: Space Physics, 115(A12).

McComas2017: McComas, D. J., Alexander, N., Allegrini, F., Bagenal, F., Beebe, C., Clark, G., ... & Dickinson, J. (2017). The Jovian auroral distributions experiment (JADE) on the Juno Mission to Jupiter. Space Science Reviews, 213 (1-4), 547-643.

Menietti2012: Menietti, J. D., Shprits, Y. Y., Horne, R. B., Woodfield, E. E., Hospodarsky, G. B., & Gurnett, D. A. (2012). Chorus, ECH, and Z mode emissions observed at Jupiter and Saturn and possible electron acceleration. Journal of Geophysical Research: Space Physics, 117 (A12).

Menietti2014: Menietti, J. D., Averkamp, T. F., Groene, J. B., Horne, R. B., Shprits, Y. Y., Woodfield, E. E., ... & Gurnett, D. A. (2014). Survey analysis of chorus intensity at Saturn. Journal of Geophysical Research: Space Physics, 119 (10), 8415-8425.

Menietti2015: Menietti, J. D., Averkamp, T. F., Ye, S. Y., Horne, R. B., Woodfield, E. E., Shprits, Y. Y., ... & Wahlund, J. E. (2015). Survey of Saturn Z−mode emission. Journal of Geophysical Research: Space Physics, 120 (8), 6176-6187.

Mihalov1998: Mihalov, J. D., H. M. Fischer, E. Pehlke, and L. J. Lanzerotti, Energetic electron measurements from the Galileo Jupiter probe, NASA/TM-1998-208756, National Aeronautics and Space Administration, December, 1998.

Nenon2017: Nénon, Q., Sicard, A., & Bourdarie, S. (2017). A new physical model of the electron radiation belts of Jupiter inside Europa's orbit. Journal of Geophysical Research: Space Physics, 122 (5), 5148-5167.

Ness1986: Ness, N. F., Acuna, M. H., Behannon, K. W., Burlaga, L. F., Connerney, J. E., Lepping, R. P., & Neubauer, F. M. (1986). Magnetic fields at Uranus. Science, 233 (4759), 85-89.

Ness1991: Ness, N. F., Connerney, J. E., Lepping, R. P., Schulz, M., & Voigt, G. H. (1991). The magnetic field and magnetospheric configuration of Uranus. uran, 739-779.

Nichols2011: Nichols, J. D. (2011). Magnetosphere−ionosphere coupling in Jupiter's middle magnetosphere: Computations including a self−consistent current sheet magnetic field model. Journal of Geophysical Research: Space Physics, 116(A10).

Nichols2015: Nichols, J. D., Achilleos, N., & Cowley, S. W. (2015). A model of force balance in Jupiter's magnetodisc including hot plasma pressure anisotropy. Journal of Geophysical Research: Space Physics, 120 (12), 10-185.

Northrop1963: Northrop, T. G. (1963). The adiabatic motion of charged particles (No. 21). Inter- science Publishers.

Paty2020: Paty, C., Arridge, C. S., Cohen, I. J., DiBraccio, G. A., Ebert, R. W., & Rymer, A. M. (2020). Ice giant magnetospheres. Philosophical Transactions of the Royal Society A, 378(2187), 20190480.

Paranicas2016: Paranicas, C., Thomsen, M. F., Achilleos, N., Andriopoulou, M., Badman, S. V., Hospodarsky, G., ... & Kollmann, P. (2016). Effects of radial motion on interchange injections at Saturn. Icarus, 264, 342-351.

Pensionerov2019: Pensionerov, I. A., Alexeev, I. I., Belenkaya, E. S., Connerney, J. E. P., & Cowley, S. W. H. (2019). Model of Jupiter's current sheet with a piecewise current density. Journal of Geophysical Research: Space Physics, 124 (3), 1843-1854.

Persoon2013: Persoon, A. M., Gurnett, D. A., Leisner, J. S., Kurth, W. S., Groene, J. B., & Faden, J. B. (2013). The plasma density distribution in the inner region of Saturn's magnetosphere. Journal of Geophysical Research: Space Physics, 118 (6), 2970-2974.

Persoon2020: Persoon, A. M., Kurth, W. S., Gurnett, D. A., Faden, J. B., Groene, J. B., Morooka, M. W., ... & Menietti, J. D. (2020). Distribution in Saturn's Inner Magnetosphere From 2.4 to 10 RS: A Diffusive Equilibrium Model. Journal of Geophysical Research: Space Physics, 125 (3), e2019JA027545.

Roederer1970: Roederer, J. G. (1970). Dynamics of geomagnetically trapped radiation. In J. G. Roederer (Ed.), Series: Physics and chemistry in space, vol. 2. Heidel- berg: Springer Berlin. doi: 10.1007/978-3-642-49300-3.

Roussos2007: Roussos, E., Jones, G. H., Krupp, N., Paranicas, C., Mitchell, D. G., Lagg, A., ... & Dougherty, M. K. (2007). Electron microdiffusion in the Saturnian radiation belts: Cassini MIMI/LEMMS observations of energetic electron absorption by the icy moons. Journal of Geophysical Research: Space Physics, 112 (A6).

Roussos2019: Roussos, E., Allanson, O., André, N., Bertucci, B., Branduardi-Raymont, G., Clark, G., ... & Gkioulidou, M. (2019). The in-situ exploration of Jupiter's radiation belts (A White Paper submitted in response to ESA's Voyage 2050 Call). arXiv preprint arXiv:1908.02339.

SantosCosta2001: Santos-Costa, D., Sault, R., Bourdarie, S., Boscher, D., Bolton, S., Thorne, R., ... & Gulkis, S. (2001). Synchrotron emission images from three-dimensional modeling of the Jovian electron radiation belts. Advances in Space Research, 28 (6), 915-918.

SantosCosta2003: Santos-Costa, D., Blanc, M., Maurice, S., & Bolton, S. J. (2003). Modeling the electron and proton radiation belts of saturn. Geophysical Research Letters, 30(20). doi: 10.1029/2003GL017972.

SantosCosta&Bolton2008: Santos-Costa, D., & Bolton, S. J. (2008). Discussing the processes constraining the jovian synchrotron radio emission’s features. Planetary and Space Science, 56(3-4), 326–345.

SantosCosta2017: Santos−Costa, D., Adumitroaie, V., Ingersoll, A., Gulkis, S., Janssen, M. A., Levin, S. M., ... & Connerney, J. E. P. (2017). First look at Jupiter's synchrotron emission from Juno's perspective. Geophysical Research Letters, 44 (17), 8676-8684.

Schippers2008: Schippers, P., Blanc, M., André, N., Dandouras, I., Lewis, G. R., Gilbert, L. K., ... & Krimigis, S. M. (2008). Multi−instrument analysis of electron populations in Saturn's magnetosphere. Journal of Geophysical Research: Space Physics, 113 (A7).

Schulz&Lanzerotti1974: Schultz, M., & Lanzerotti, L. (1974). Particle diffusion in the radiation belts, phys. and chem. Space, 7.

Schulz&McNab1996: Schulz, M., & McNab, M. C. (1996). Source−surface modeling of planetary magnetospheres. Journal of Geophysical Research: Space Physics, 101 (A3), 5095-5118.

Selesnick1991: Selesnick, R. S., & Stone, E. C. (1991). Energetic electrons at Uranus: Bimodal diffusion in a satellite limited radiation belt. Journal of Geophysical Research: Space Physics, 96 (A4), 5651-5665.

Shprits2012: Shprits, Y. Y., Menietti, J. D., Gu, X., Kim, K. C., & Horne, R. B. (2012). Gyroresonant interactions between the radiation belt electrons and whistler mode chorus waves in the radiation environments of Earth, Jupiter, and Saturn: A comparative study. Journal of Geophysical Research: Space Physics, 117 (A11).

Sicard2004: Sicard, A., & Bourdarie, S. (2004). Physical Electron Belt Model from Jupiter's surface to the orbit of Europa. Journal of Geophysical Research: Space Physics, 109 (A2).

Voigt1983: Voigt, G. H., Hill, T. W., & Dessler, A. J. (1983). The magnetosphere of Uranus-Plasma sources, convection, and field configuration. The Astrophysical Journal, 266, 390-401.

Voigt1986: Voigt, G. H. (1986). Field line twist and field−aligned currents in an axially symmetric equilibrium magnetosphere. Journal of Geophysical Research: Space Physics, 91 (A10), 10995-11002.

Voigt1987: Voigt, G. H., Behannon, K. W., & Ness, N. F. (1987). Magnetic field and current structures in the magnetosphere of Uranus. Journal of Geophysical Research: Space Physics, 92 (A13), 15337-15346.

Woodfield2014: Woodfield, E. E., Horne, R. B., Glauert, S. A., Menietti, J. D., & Shprits, Y. Y. (2014). The origin of Jupiter's outer radiation belt. Journal of Geophysical Research: Space Physics, 119 (5), 3490-3502.

Woodfield2018: Woodfield, E. E., Horne, R. B., Glauert, S. A., Menietti, J. D., Shprits, Y. Y., & Kurth, W. S. (2018). Formation of electron radiation belts at Saturn by Z-mode wave acceleration. Nature communications, 9 (1), 1-7.

Woodfield2019: Woodfield, E. E., Glauert, S. A., Menietti, J. D., Averkamp, T. F., Horne, R. B., & Shprits, Y. Y. (2019). Rapid electron acceleration in low−density regions of Saturn's radiation belt by whistler mode chorus waves. Geophysical research letters, 46 (13), 7191-7198.

Woodfield2020: Woodfield, E. E., Glauert, S. A., Menietti, J. D., Horne, R. B., & Shprits, Y. (2020, December). The Unusual Effect of Hiss Waves on Electrons in Saturn’s Radiation Belts. In AGU Fall Meeting 2020. AGU (SM014-06).

Young2004: Young, D. T., Berthelier, J. J., Blanc, M., Burch, J. L., Coates, A. J., Goldstein, R., ... & McComas, D. J. (2004). Cassini plasma spectrometer investigation. In The Cassini-Huygens Mission (pp. 1-112). Springer, Dordrecht.

Yu2019: Yu, J., Li, L. Y., Cui, J., Cao, J. B., & Wang, J. (2019). Combined effects of equatorial chorus waves and high−latitude Z−mode waves on Saturn's radiation belt electrons. Geophysical Research Letters, 46 (15), 8624-8632.